iScience

CellPress
OPEN ACCESS

Article

Suppression of the *KRAS-NRF2* axis shifts arginine into the phosphocreatine energy system in pancreatic cancer cells

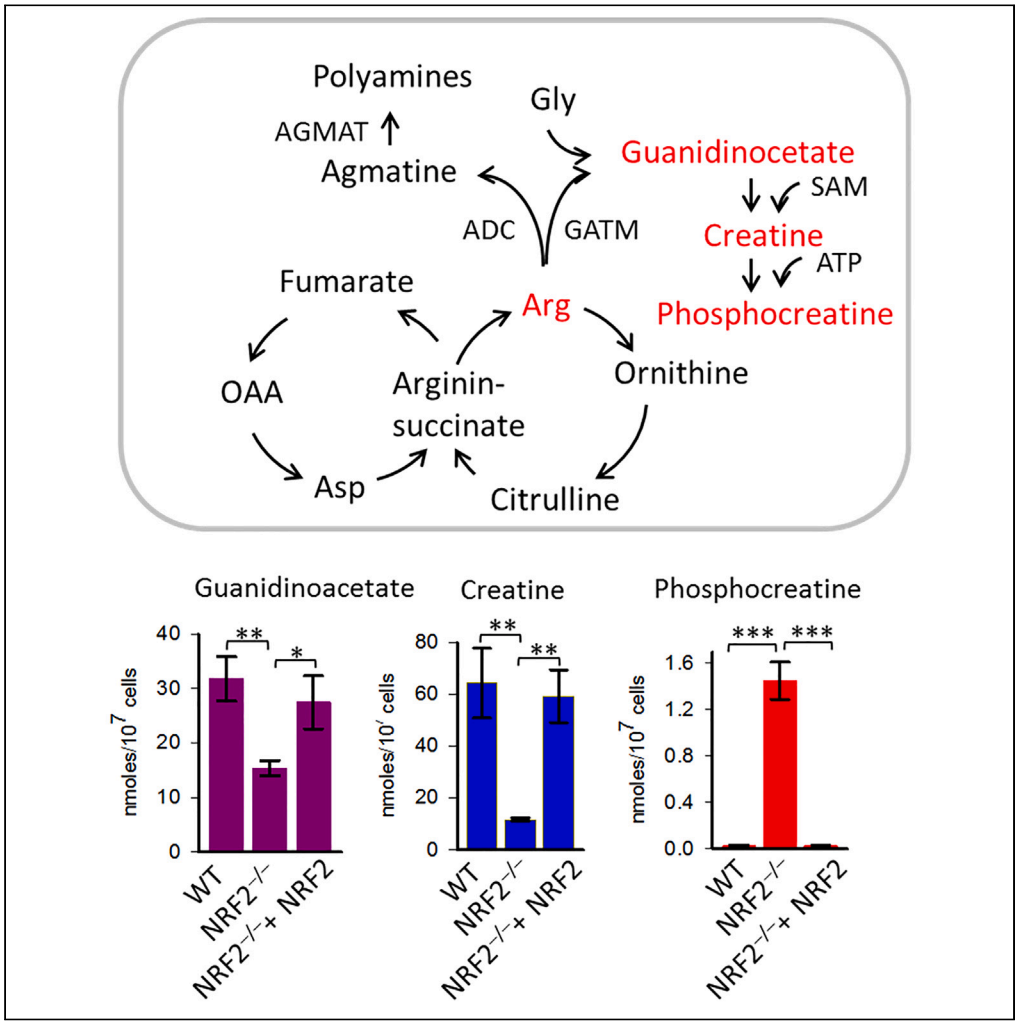

Eros Di Giorgio, Himanshi Choudhary, Annalisa Ferino, ..., Marina Comelli, Valentina Rapozzi, Luigi E. Xodo

eros.digiorgio@uniud.it (E.D.G.)
luigi.xodo@uniud.it (L.E.X.)

Highlights

The *KRAS-NRF2* axis controls redox homeostasis and metabolism in PDAC cells

Suppression of *KRAS-NRF2* channels arginine towards phosphocreatine and polyamines

Blockade of arginine metabolism inhibits the growth of 3D PDAC spheroids

Co-targeting of *KRAS/NRF2* and creatine pathway is more effective than monotherapies

Di Giorgio et al., iScience *26*, 108566
December 15, 2023
https://doi.org/10.1016/j.isci.2023.108566

iScience

CellPress
OPEN ACCESS

Article

Suppression of the *KRAS-NRF2* axis shifts arginine into the phosphocreatine energy system in pancreatic cancer cells

Eros Di Giorgio,[1,2,3,*] Himanshi Choudhary,[1,2] Annalisa Ferino,[1] Ylenia Cortolezzis,[1] Emiliano Dalla,[1] Francesca D'Este,[1] Marina Comelli,[1] Valentina Rapozzi,[1] and Luigi E. Xodo[1,*]

SUMMARY

In pancreatic ductal adenocarcinomas (PDAC), the *KRAS*^{G12D}-*NRF2* axis controls cellular functions such as redox homeostasis and metabolism. Disruption of this axis through suppression of *NRF2* leads to profound reprogramming of metabolism. Unbiased transcriptome and metabolome analyses showed that PDAC cells with disrupted *KRAS*^{G12D}-*NRF2* signaling (*NRF2*$^{-/-}$ cells) shift from aerobic glycolysis to metabolic pathways fed by amino acids. Metabolome, RNA-seq and qRT-PCR analyses revealed a blockade of the urea cycle, making *NRF2*$^{-/-}$ cells dependent on exogenous arginine for survival. Arginine is channeled into anabolic pathways, including the synthesis of phosphocreatine, which generates an energy buffer essential for cell growth. A similar switch was observed in tumor clones that had survived FOLFIRINOX therapy or blockade of *KRAS* signaling. Inhibition of the creatine pathway with cyclocreatine reduced both ATP and invasion rate in 3D spheroids from *NRF2*-deficient PDAC cells. Our study provides basis for the rational development of combination therapies for pancreatic cancer.

INTRODUCTION

Pancreatic ductal adenocarcinoma (PDAC) is estimated to become the second cause of cancer-related death in Western countries by 2030.[1] The 5-year survival rate of PDAC patients is 12%, as the disease is often diagnosed at an advanced stage and develops resistance to conventional chemotherapy.[2] A wide range of genetic alterations are present in PDAC including activating point mutations in the *KRAS* proto-oncogene and loss-of-function mutations in tumor suppressor genes, such as *TP53*, *CDNK2A*, *DPC4*/*SMAD4*, and *BRCA2*.[3] Missense mutations in *KRAS* – exon 1, codon 12, 13 and 61– are present in >95% of PDAC cases.[4] These mutations lock the RAS protein in the active GTP-bound state which constitutively stimulates cancer growth. The role of oncogenic *KRAS* in pancreatic tumorigenesis has been the subject of investigation for many years. Hingorani et al.[5] reported that the endogenous expression of *KRAS*^{G12D} in mouse pancreatic cells results in ductal lesions as occur in human pancreatic intraepithelial neoplasia giving rise to invasive pancreatic cancer. Recent studies demonstrated that *KRAS*^{G12D} is required in all stages of the PDAC carcinogenesis, although progression to metastatic cancer requires the acquisition of additional genetic alterations, such as mutation of *TP53*.[6] *KRAS*^{G12D} plays a preeminent role in the development of PDAC as suggested by the fact that the inactivation of this oncogene by genetic tools results in the reversion of the carcinogenesis.[7] Transcriptomic and metabolomic studies have demonstrated that *KRAS*^{G12D} is a key regulator of the metabolic reprogramming occurring in PDAC cells to fuel an increased demand of nutrients by highly proliferating cells. Under the action of constitutively active *KRAS*^{G12D}, pancreatic cancer cells acquire a glycolytic phenotype characterized by a high glycolytic flux: a metabolic condition known as the Warburg effect.[8] This high glycolytic flux channels intermediates into anabolic pathways to satisfy the requirements of biomass and reducing power of cancer cells.[9] Recent studies have reported that *NRF2*, the master regulator of oxidative stress in the cell,[10] is upregulated by *KRAS* in PDAC cells, suggesting that *KRAS* is involved in the regulation of the redox homeostasis in pancreatic cancer.[11,12] *NRF2* seems to have also ROS-independent functions because it has been reported that is essential for the growth of human tumor organoids and tumor xenografts in athymic nude mice, in the absence of DNA damage.[13] In fact, evidence that *NRF2* promotes pancreatic tumor maintenance by redirecting glucose and glutamine into anabolic pathways has been provided.[14] In a previous work we have reported the in Panc-1 cells (*KRAS*^{G12D}, TP53 mutated) *KRAS*^{G12D} and *NRF2* form an axis that controls cell growth.[12,15] The mechanism by which oncogenic *KRAS* rewires the metabolism in PDAC and the role played by *NRF2* in the process is not yet defined. In this study, we have used a transcriptomic and metabolomic approach to investigate the impact of the *KRAS*^{G12D}-*NRF2* axis on the metabolism of PDAC cells. We found that suppression of the *KRAS*^{G12D}-*NRF2* axis by deletion of *NRF2* leads to a cellular phenotype in which the urea cycle is blocked and heavily dependent on exogenous arginine, which increases the level of phosphocreatine, a

[1]Department of Medicine, Laboratory of Biochemistry, P.le Kolbe 4, 33100 Udine, Italy
[2]These authors contributed equally
[3]Lead contact
*Correspondence: eros.digiorgio@uniud.it (E.D.G.), luigi.xodo@uniud.it (L.E.X.)
https://doi.org/10.1016/j.isci.2023.108566

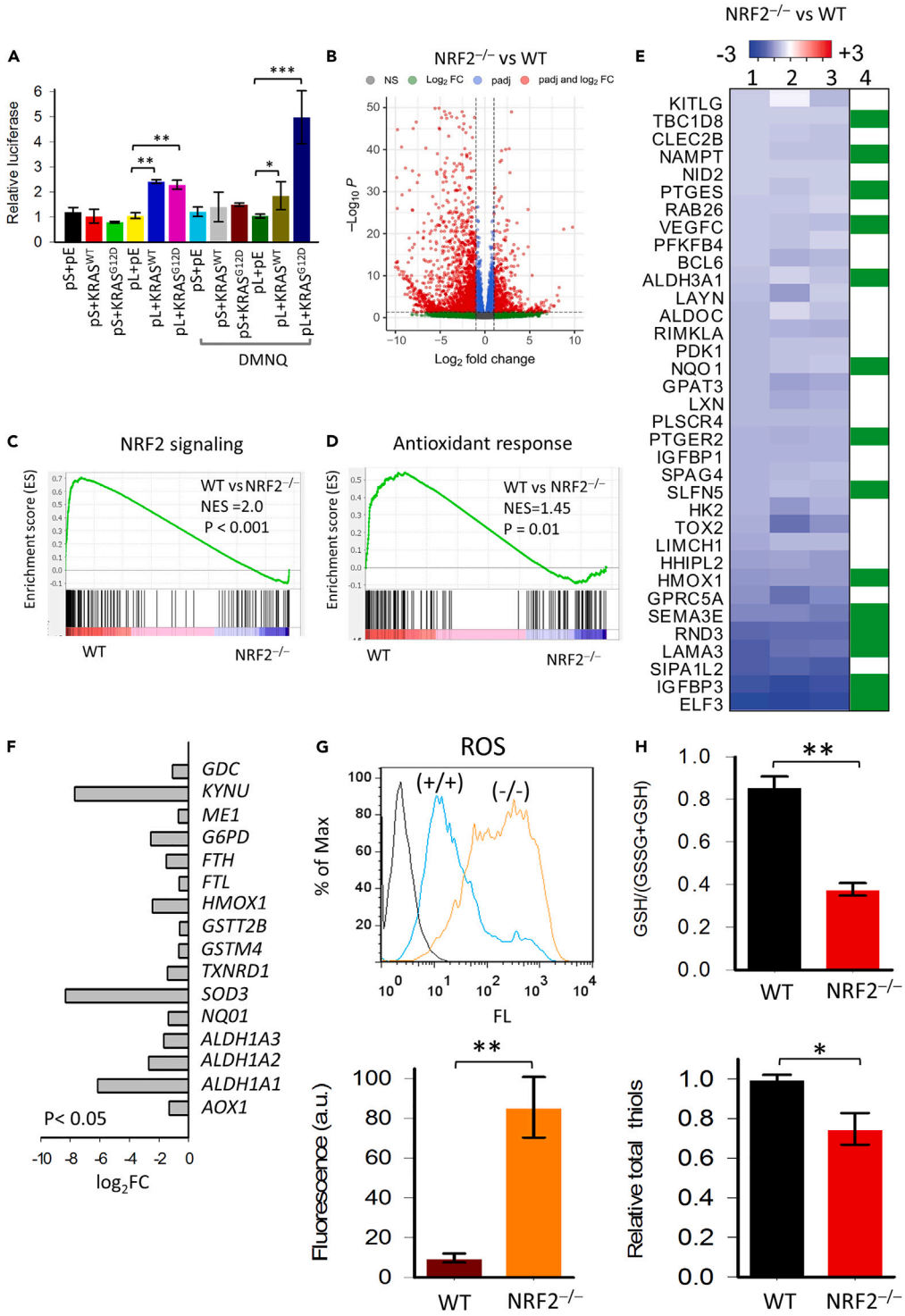

Figure 1. Characterization of Panc-1 *NRF2*$^{-/-}$ cells

(A) Luciferase driven by the full (pL) or truncated (pS) NRF2 promoter after ectopic expression of wild-type KRAS or KRASG12D. DMNQ, 1,4-naphthoquinone, is a molecule that produces ROS.

(B) Volcano plot of DEGs in *NRF2*$^{-/-}$ compared to WT-Panc-1 cells.

(C and D) Gene Set Enrichment Analysis (GSEA) plots showing the enrichment of NRF2 signaling and antioxidant response genes in WT versus *NRF2*$^{-/-}$ Panc-1 cells.

Figure 1. *Continued*

(E) Heatmap showing fold expression of NRF2 signaling in NRF2$^{-/-}$ Panc-1 cells compared to WT cells; genes directly regulated by NRF2 through direct binding to the proximal promoter are marked in green (lane 4).

(F) Log_2 (fold change) of major DEGs ($p < 0.05$).

(G) Level of basal ROS in *NRF2*$^{-/-}$ and WT Panc-1 cells.

(H) GSH/total glutathione and total thiol groups in *NRF2*$^{-/-}$ and WT Panc-1 cells; Data represent the mean ± s.d. of at least 3 independent experiments: *$p \leq 0.05$; **$p \leq 0.01$; ***$p \leq 0.001$ by Student's *t* test.

vital energy reserve for the cell.[16] Phosphocreatine is a phosphagenic energy storage compound found primarily in muscle and nerve tissue, but has recently been reported to play a role in cancer as well.[17,18] As PDAC cells deficient in the *KRAS*^{G12D}-*NRF2* axis become highly dependent on exogenous arginine, the use of combined therapies targeting both *KRAS* signaling and arginine metabolism may provide important therapeutic options for PDAC patients.

RESULTS

Generation and characterization of Panc-1 *NRF2*$^{-/-}$ cells deficient of the *KRAS-NRF2* axis

To examine the differential expression of *NRF2* between normal and tumor tissues in PDAC patients, we interrogated GSE15471, a publicly available microarray dataset. The database shows that *NRF2* is 3-fold more expressed in PDAC than in tumor-surrounding normal tissues ($p \leq 0.0002$). Kaplan–Meier plots show that PDAC patients with high *NRF2* expression exhibit a lower survival probability than patients with a low *NRF2* expression ($p = 0.0016$) (Figure S1A), suggesting that a highly expressed *NRF2* is associated with a poor prognosis. An elegant metabolomic work by DePinho et al. reported that advanced PDAC strictly depends on *KRAS*^{G12D}, as the oncogene reprograms glucose and glutamine metabolism.[9,19] However, how *KRAS*^{G12D} controls cancer metabolism is still a matter of investigation. The discovery that *KRAS*^{G12D} is tightly connected with *NRF2*,[11,12,20] with which it forms an axis controlling several cellular functions, suggests that the metabolic reprogramming induced by *KRAS*^{G12D} could be mediated, in part or entirely, by *NRF2*. To address this question, we compared the metabolism of normal Panc-1 cells carrying the *KRAS*^{G12D} mutation[21] with that of Panc-1 cells in which the *KRAS*^{G12D}-*NRF2* axis was completely inactivated by deletion of *NRF2* with CRISPR-Cas9. We could not inactivate the axis by suppressing *KRAS*^{G12D} because the cells are addicted to it and do not survive when the oncogene is inhibited. We isolated two knockout (KO) clones, in which both *NRF2* alleles bear frameshift mutations causing the deletion of the gene. We found in clone KO-134 deletions of 2 and 10 nt in the *NRF2* alleles, whereas in KO-16 deletions of 1 and 2 nt (Figure S1B). We measured the level of protein NRF2 by western blot and found that it was indeed expressed in WT but not in the KO cells. From now on we called the latter *NRF2*$^{-/-}$ cells (Figure S1C). As a functional control, we tested the expression of luciferase driven by the *NQO1* promoter bearing the antioxidant response element (ARE) recognized by NRF2. As a functional control, we tested the expression of luciferase driven by the *NQO1* promoter carrying the antioxidant response element (ARE) recognized by NRF2. While luciferase was expressed in WT cells that also respond to NRF2 activators and inhibitors, it was not expressed in *NRF2*$^{-/-}$ cells, as expected (Figure S1D). The direct link between oncogenic *KRAS* and *NRF2* was proven by the fact that the ectopic expression of *KRAS*^{G12D} in Panc-1 cells causes a clear increase of *NRF2*.[12] An insight into the *KRAS*^{G12D}-*NRF2* axis was obtained by engineering two expression vectors, pL and pS (see STAR Methods). Vector pL bears the full-length *NRF2* promoter, with ARE-like elements at −754 and −492, upstream of *Firefly* luciferase. In contrast, vector pS bore a *NRF2* promoter lacking AREs. We found that the ectopic expression of mutant *KRAS*^{G12D} or wild-type (WT) *KRAS* increased by 2-fold luciferase from pL but not from pS, showing that *KRAS* upregulates *NRF2* and that the ARE-like elements are essential for its activation (Figure 1A). When the cells were transfected with *KRAS*^{G12D} and treated with 1,4 naphthoquinone (DMNQ), a molecule that produces ROS,[22] luciferase driven by pL increased up to 5-fold. Together, ROS and *KRAS* induce a stronger upregulation of *NRF2*, probably through *MAPK/ERK* signaling (Figure S1E), as previously suggested.[23,24] In addition, we found that the suppression of *KRAS* expression with siRNA caused the simultaneous downregulation of *NRF2*, confirming a close link between oncogenic *KRAS* and *NRF2* (Figure S1F). Finally, GSE15471 data from PDAC patients support the notion that *KRAS*^{G12D} and *NRF2* are crucial for PDAC, as the Kaplan-Meier plot of patients with high expression of both *KRAS*^{G12D} and *NRF2* showed a significantly lower probability of survival than patients with lower expression of the genes ($p = 0.00012$) (Figures S2A and S2B). Moreover, the levels of *KRAS* and *NRF2* mRNAs show a positive mutual correlation in PDAC patients (Figure S2C).

To evaluate the effects of the *KRAS*^{G12D}-*NRF2* axis in PDAC, we performed transcriptomic and metabolomic analyses on WT Panc-1 cells (with an active *KRAS*^{G12D}-*NRF2* axis) and *NRF2*$^{-/-}$ Panc-1 cells (with a silent *KRAS*^{G12D}-*NRF2* axis).

Transcriptome analysis of Panc-1 cells following the suppression of the *KRAS* ^{G12D}-*NRF2* axis

The transcriptional changes induced by the suppression of the *KRAS* ^{G12D}-*NRF2* axis in Panc-1 cells were determined by RNA-seq analysis on WT and *NRF2*$^{-/-}$ cells. Differentially expressed genes (DEGs) between *NRF2*$^{-/-}$ and WT cells are shown by the principal component analysis (PCA) (Figure S3A). PCA displays a high reproducibility of the sample replicates and significant variation between WT and *NRF2*$^{-/-}$ cells. Among the transcripts, a cluster of 1888 DEGs is downregulated and a cluster of 666 DEGs is upregulated in *NRF2*$^{-/-}$ cells compared to WT cells, according to a threshold $|\log_2 FC| \geq 1$, Padj.< 0.05. These data suggest that the suppression of the *KRAS* ^{G12D}-*NRF2* axis has a strong impact on the transcriptome of Panc-1 cells. The data are summarized by a heatmap of DEGs (Figur S3B) and a volcano plot (Figure 1B). An unbiased gene set enrichment analysis (GSEA) revealed, as expected, a striking impairment of KEGG-defined pathways relative to *NRF2* signaling (GSE94393) ($p < 0.0001$) and the antioxidant response to oxidative stress (M5968) ($p < 0.01$) in *NRF2*$^{-/-}$ cells (Figures 1C and 1D).

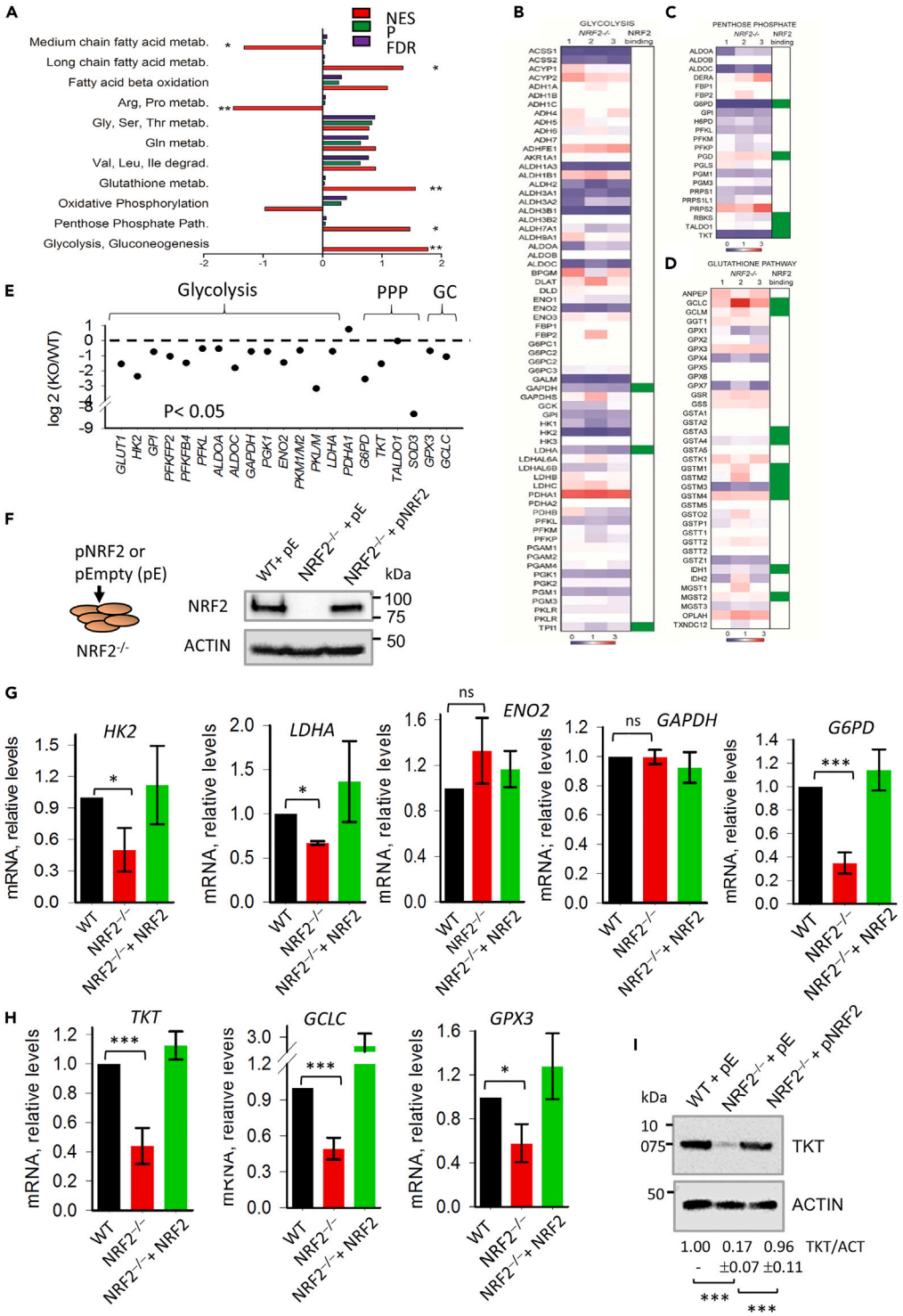

Figure 2. NRF2 depletion affects Panc-1 transcriptome and promotes a deep metabolic reprogramming

(A) Functional enrichment analysis of WT cells compared to *NRF2*$^{-/-}$ cells. NES = normal enrichment score, FDR = false discovery rate, p= p-value.

(B–D) Heatmaps of DEGs relative to glycolysis, PPP and glutathione pathways.

(E) DEGs of enzymes involved in glycolysis, PPP and glutathione cycle pathways.

Figure 2. *Continued*

(F–H) Expression level of some key enzymes involved in the pathways determined by qRT-PCR. To demonstrate that the enzymes are controlled by the *KRAS*^{G12D}-*NRF2* axis, we re-expressed *NRF2* in *NRF2*$^{-/-}$ cells and obtained an expression profile similar to that of WT cells.

(I) Western blot showing the level of tkt in WT, *NRF2*$^{-/-}$ and *NRF2*$^{-/-}$ cells in which *NRF2* was re-expressed. Data represent the mean ± s.d. of at least 3 independent experiments: *p ≤ 0.05; **p ≤ 0.01; ***p ≤ 0.001 by Student's *t* test.

Downregulated DEGs associated to *NRF2* are shown in the heatmap of Figure 1E. The genes that are directly targeted by NRF2 are marked in green in the right column of the heatmap. As expected, the key genes involved in the maintenance of the redox homeostasis are downregulated in NRF2$^{-/-}$ cells: *AOX1*, *ALDH3A1*, *NQO1*, *HMOX1*, *TXNRD1*, *GST*, *GCLC* and *SOD3* (Figure 1F). As the antioxidant response coordinated by *NRF2* in response to an increase of oxidative stress is lost in NRF2$^{-/-}$ cells, the basal level of ROS, measured by flow cytometry, was indeed found ~ 8-fold higher than in WT cells (Figure 1G). We also found that the ratio between reduced and total glutathione was 0.88 in WT and 0.4 in NRF2$^{-/-}$ cells, and the total cellular amount of reduced thiols was ~25% lower in *NRF2*$^{-/-}$ compared to WT cells (Figure 1H). Collectively, our data show that the suppression of the *KRAS*^{G12D}-*NRF2* axis strongly affects the redox homeostasis in pancreatic cancer cells. Despite this, we found that *NRF2*-deficient cells showed a proliferation rate only ~25% lower than that of WT cells, over 11 days of observation (Figure S3C).

The *KRAS* ^{G12D}-*NRF2* axis controls the metabolic reprogramming in PDAC cells

We interrogated clusterProfiler to carry out a functional enrichment analysis of DEGs to reveal enrichment of specific metabolic pathways (Figure 2A). The analysis evidenced a strong and statistically significant decline of glycolysis, pentose phosphate pathway (PPP), glutathione cycle and long-chain fatty acid metabolism and a simultaneous deep reactivation of arginine/proline and medium-chain fatty acid metabolism in *NRF2*$^{-/-}$ cells compared to WT cells. The heatmaps relative to glycolysis, PPP and glutathione cycle are reported in Figures 2B–2D. Consistent with gene microarray data of two GEO datasets which showed that glycolysis, PPP and GSH are upregulated in *NRF2*-active esophagus cells,[25] we found that the suppression of the *KRAS*^{G12D}-*NRF2* axis in Panc-1 cells results in the downregulation ($p < 0.05$) of glycolytic (*HK2*, *GPI*, *PFKL*, *ALDOA/C*, *TPI1*, *PGK1*, *ENO2*, *PKM1/2*, and *LDHA*), PPP (*G6PD*, *TALDO1*, and *TKT*), glutathione cycle (*GCLC* and *GPX4*) and glucose translocase (*GLUT1)* genes (Figures 2E and S3D). Since *KRAS*^{G12D} controls *NRF2*, our data are in keeping with those of DePinho et al. who reported that *KRAS*^{G12D} regulates glucose metabolism in PDAC.[9] Moreover, the knockdown of *NRF2* by siRNA in A549 lung cancer cells resulted in a decrease in key PPP enzymes (G6PD and TKT)[14] and glutathione synthesis (GCLC),[26] in agreement with our data. However, despite the low glycolytic flux, *NRF2*$^{-/-}$ cells show a proliferation rate that is only 25% lower than that of WT cells, suggesting that the cells use for growth substrates other than glucose, such as amino acids, especially arginine, and medium-chain fatty acids. To confirm the RNA-seq data, we measured by qRT-PCR the expression level of genes encoding for key glycolytic, PPP and glutathione enzymes. In addition, to unambiguously prove that the metabolic rewiring occurring in PDAC cells is strictly linked with *NRF2*, we carried out also rescue experiments. We reasoned that the constitutive re-expression of *NRF2* in *NRF2*$^{-/-}$ cells (with plasmid pWZL-Neo NRF2, called pNRF2 in Figure 2F) should reconstitute the *KRAS*^{G12D}-*NRF2* axis and thus the metabolic features typical of WT cells. As far as we know, *NRF2* rescue experiments have not been done before and show for the first time that *NRF2* mediates the metabolic reprogramming in pancreatic cancer cells. In agreement with RNA-seq data, qRT-PCR showed that glycolytic *HK2* and *LDHA* were indeed ~50% downregulated in *NRF2*$^{-/-}$ ($p < 0.05$). Notably, their levels were completely rescued when *NRF2* was re-expressed in NRF2$^{-/-}$ cells. In contrast, *ENO2* and *GAPDH* show little dependence on *NRF2* (Figures 2G and 2H). Also, the two genes encoding for key enzymes of PPP, *G6PD* and *TKT*, were found strongly downregulated in *NRF2*$^{-/-}$ cells ($p < 0.05$), in agreement with RNA-seq. The downregulation of *TKT* in *NRF2*$^{-/-}$ cells was also confirmed at protein level (Figure 2I). Interestingly, also the level of the PPP genes (*G6PD, TKT*) were completely restored when the *KRAS*^{G12D}-*NRF2* axis was re-established in *NRF2*$^{-/-}$ cells (Figures 2H and 2I). A similar result was observed with the genes involved in the glutathione cycle (*GCLC* and *GPX3*) (Figure 2H). In general, the qRT-PCR data were in excellent agreement with those obtained with RNA-seq.

Panc-1 NRF2$^{-/-}$ cells show higher mitochondrial function and a change in oncogenic program

We performed Seahorse XF Cell Mito Stress Test to examine the metabolic adjustment occurring in *NRF2*$^{-/-}$ cells and performed also *NRF2*-rescue experiments as a control. The results are summarized in Table S1. Figures 3A–3C reports a typical real-time oxygen consumption rate (OCR) profile obtained with the classical protocol of three different injections: oligomycin, FCCP, and rotenone/ antimycin A. The basal respiration in NRF2$^{-/-}$cells was 2-fold higher than in WT cells, in keeping with RNA-seq data suggesting that the former cells are less glycolytic and more dependent on aerobic metabolism. By using the ATP-synthase inhibitor oligomycin, the ATP-linked respiration was 5.2 ± 0.7 and 11.3 ± 1.1 pmol/min·μg in WT and *NRF2*$^{-/-}$ cells, respectively. Interestingly, when *NRF2* was re-expressed in *NRF2*$^{-/-}$ cells, the ATP-linked respiration fell to 5.7 ± 1.2 pmol/min·μg, as the cells restored the glycolytic phenotype typical of WT cells. The successive addition of uncoupler FCCP showed that the maximal respiratory rate in *NRF2*$^{-/-}$ cells was 3-fold higher than in WT cells. The addition of rotenone/antimycin A showed that basal respiration over non-mitochondrial oxygen consumption was 1.5 in WT cells and ~2.1 in *NRF2*$^{-/-}$ cells, confirming that the former is more glycolytic than the latter. The OCR-ECAR (bioenergetic profile) plot shows, indeed, that *NRF2*$^{-/-}$ cells display less glycolysis and more oxidative phosphorylation than WT cells (Figure S4A). Indeed, the OCR/ECAR ratio is lower in WT cells (1.5) compared to *NRF2*$^{-/-}$ cells (3.7), as expected (Figure 3C). Consistent with this, *NRF2*$^{-/-}$ cells show more sensitivity to the OXPHOS inhibitor phenformin than WT cells (Figures S4B and S4C). Notably, the respiratory parameters fall to normal levels in *NRF2*-rescue cells, clearly demonstrating that the mitochondrial metabolism is controlled by the *KRAS*^{G12D}-*NRF2* axis. It also controls the redox homeostasis as the ROS level in *NRF2*$^{-/-}$ cells drop to levels as in WT cells

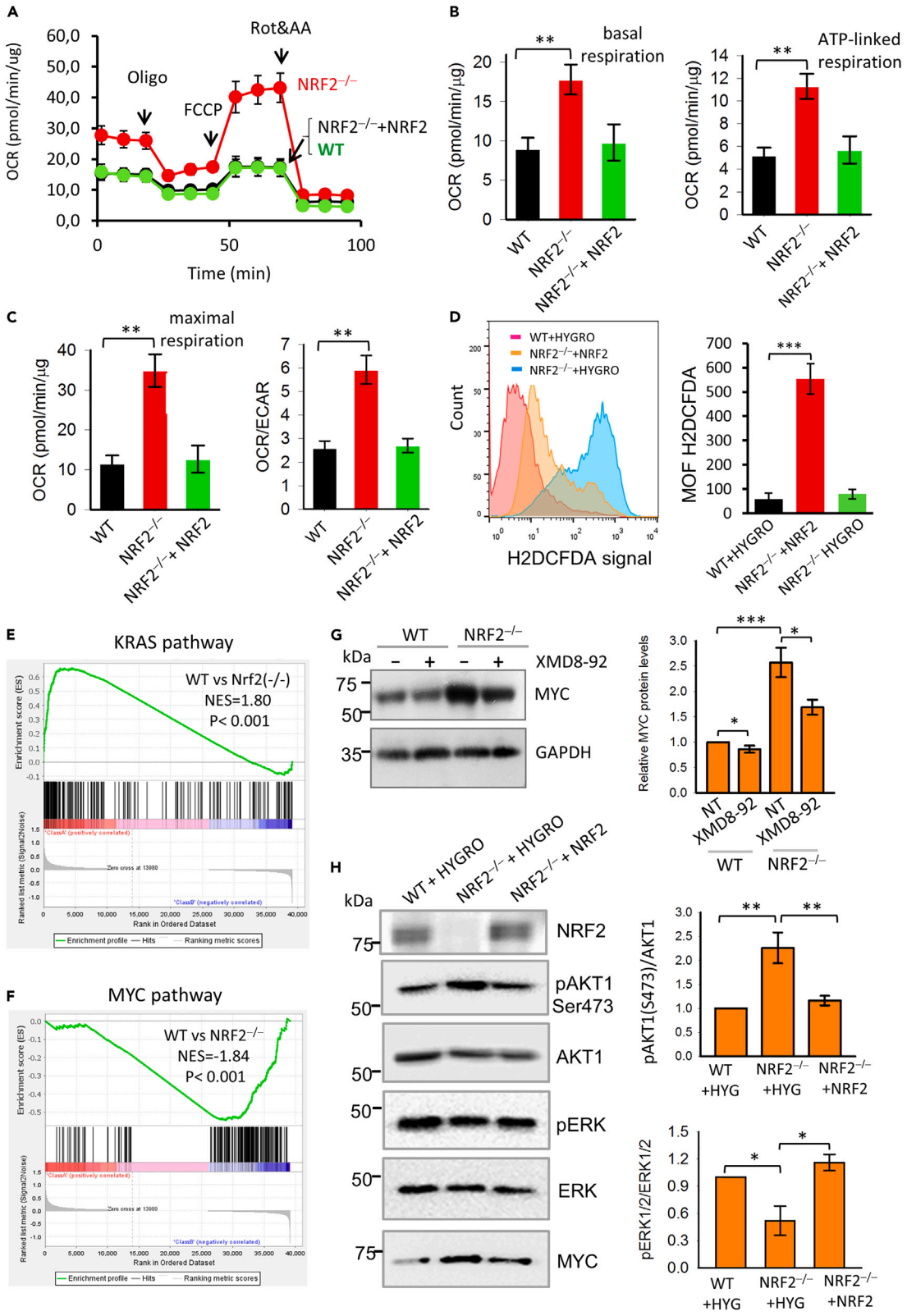
A
OCR (pmol/min/ug)
Oligo
FCCP
Rot&AA
NRF2−/−
NRF2−/−+NRF2
WT
Time (min)
B
basal respiration
ATP-linked respiration
OCR (pmol/min/µg)
WT
NRF2−/−
NRF2−/−+ NRF2
C
maximal respiration
OCR/ECAR
D
WT+HYGRO
NRF2−/−+NRF2
NRF2−/−+HYGRO
Count
H2DCFDA signal
MOF H2DCFDA
WT+HYGRO
NRF2−/− +NRF2
NRF2−/− HYGRO
E
KRAS pathway
WT vs Nrf2(-/-)
NES=1.80
P< 0.001
Enrichment score (ES)
Ranked list metric (Signal2Noise)
Rank in Ordered Dataset
Enrichment profile
Hits
Ranking metric scores
F
MYC pathway
WT vs NRF2−/−
NES=-1.84
P< 0.001
G
WT
NRF2−/−
kDa
XMD8-92
MYC
GAPDH
Relative MYC protein levels
NT
XMD8-92
H
WT + HYGRO
NRF2−/− + HYGRO
NRF2−/− + NRF2
NRF2
pAKT1 Ser473
AKT1
pERK
ERK
MYC
pAKT1(S473)/AKT1
pERK1/2/ERK1/2
+HYG

Figure 3. Panc-1 *NRF2*$^{-/-}$ cells show higher mitochondrial function and a change in oncogenic program

(A) Real-time oxygen consumption rate (OCR) was determined during successive treatments with oligomycin (ATP synthase inhibitor), FCCP (uncoupler of oxidative phosphorylation), rotenone (complex I inhibitor) and antimycin-A (complex III inhibitor) in WT, *NRF2*$^{-/-}$ and *NRF2*$^{-/-}$ +NRF2 cells.

(B and C) The rates of basal respiration, ATP-coupled respiration, maximal respiration and OCR/ECAR ratio in NRF2$^{-/-}$ and *NRF2*$^{-/-}$ +NRF2 cells were normalised to total protein content and quantified.

(D) *NRF2*$^{-/-}$ cells show a 10-fold higher ROS level than WT cells. When NRF2 is re-expressed in the cells, the ROS level decreases to the level observed in WT cells.

(E and F) GSEA plots showing the enrichment of KRAS in WT and MYC in *NRF2*$^{-/-}$ Panc-1 cells.

(G) Expression of MYC in WT and *NRF2*$^{-/-}$ cells; XMD8-92 (5 μM) was used to inhibit ERK5 for 24 h. Densitometric analysis of 3 experiments is provided.

(H) phosphorylation levels of AKT1 and ERK1/2 in WT, *NRF2*$^{-/-}$ and *NRF2*$^{-/-}$ + NRF2 cells. Densitometric analysis of 4 experiments is provided; data represent the mean ± s.d. of at least 3 independent experiments: *p ≤ 0.05; **p ≤ 0.01; ***p ≤ 0.001 by Student's *t* test.

when *NRF2* is re-expressed (Figure 3D). Another interesting finding was obtained with GSEA which showed that in NRF2$^{-/-}$ cells the *KRAS* signaling is switched off, while the *MYC* signaling is switched on (Figures 3E and 3F). This may suggest that the malignancy of *NRF2*$^{-/-}$ cells is maintained by a change in the oncogenic program. According to ClueGO, the RAS-GEF pathway promoting the RAS nucleotide exchange for RAS activation is dramatically downregulated in *NRF2*$^{-/-}$ cells, consistent with an impairment of the *KRAS* signaling in *NRF2*$^{-/-}$ cells. We found a significant increase (~2.5-fold) in the level of MYC protein in *NRF2*$^{-/-}$ cells compared to WT cells. The inhibition of ERK5 by XMD8-92 decreased MYC protein in *NRF2*$^{-/-}$ cells (Figure 3G), suggesting that the collateral activation of ERK5 may be responsible for the stabilization of MYC, as previously observed in PDAC.[27] Overall, *NRF2*$^{-/-}$ cells are characterized by partial dephosphorylation of ERK1/2, increased activation of the AKT1 pathway and upregulation of MYC (Figure 3H). The activation of PI3K/AKT and MYC mitogenic pathways could compensate for the partial blockade of the MAPK pathway observed in KO cells, as observed in other contexts.[28]

Panc-1 cells respond to the suppression of the *KRAS*^{G12D}*-NRF2* axis by activating anabolic pathways fed by arginine

Pathway enrichment analyses showed that *NRF2*$^{-/-}$ cells respond to their limited capacity to use glucose by up-regulating key enzymes of arginine/proline and medium-chain fatty acid metabolism (Figure 2A). We decided to focus on arginine metabolism. Arginine is not only a key component of the urea cycle (UC), but can also support the biosynthesis of phosphocreatine and nitric oxide. It also contribute to the biosynthesis of polyamines along with glutamine (Figures 4A–4D).[29,30] Arginine is a non-essential amino acid that can be synthesized from citrulline and aspartate via *argininosuccinate synthetase* (ASS1): the rate-limiting enzyme of the pathway.[31] As ASS1 is downregulated in *NRF2*$^{-/-}$ Panc-1 cells together with *argininosuccinate lyase* (*ASL*) and *ornithine transcarbamylase* (*OTC*), the production of endogenous arginine in *NRF2*$^{-/-}$ cells is expected to be low, and the cells should become arginine-auxotrophic and dependent on the uptake of arginine from the extracellular environment. Arginine is taken up by pancreatic cancer cells via the y+L transport system (encoded by the *SLC3A* and *SLC7A* genes).[32] We found that in *NRF2*$^{-/-}$ Panc-1 cells, *SLC7A6*, which transports both arginine and ornithine, is overexpressed. The *SLC7A2* isoform has been linked to the prognosis of PDAC patients.[33] The fate of exogenous arginine in pancreatic cancer cells lacking the *KRAS*^{G12D}*-NRF2* axis is not related to UC, but to anabolic pathways that promote cell growth under conditions where glucose consumption is reduced.[29] The first non-UC enzyme acting on arginine is *arginine-glycine amidinotransferase* (GATM), which produces guanidinoacetate: a metabolite from which creatine is formed. Creatine is then phosphorylated by *creatine kinase* (CKB) to phosphocreatine,[17] which forms a temporal energy reserve in the form of energy-rich phosphate bonds that can be rapidly mobilized when cells have an increased energy demand.[18,34] *Arginase* 1 (*ARG1*) is strongly downregulated in *NRF2*$^{-/-}$ cells, consistent with the reduced utilization of arginine in UC, whereas *ARG2*, which is expressed in non-hepatic tissues, including cancer,[35] is significantly upregulated. Arginine is converted to ornithine by ARG2 and, together with glutamine,[27] contributes to the synthesis of polyamines in PDAC.[36] Two other enzymes can metabolize arginine: *nitric oxide synthase* (NOS) and *agmatinase* (AGMAT). The former produces nitric oxide, a gaseous signaling molecule that regulates various processes, including the progression of cancer,[37] the latter produces agmatine, which leads to polyamines.[38] Our RNA-seq data show that genes encoding enzymes of the creatine, polyamine and nitric oxide pathways are upregulated in NRF2$^{-/-}$ cells (Figure 4D). Interestingly, we found that *carbamoyl phosphate synthase 1* (*CPS1*), which encodes an enzyme that catalyzes the synthesis of carbamoyl phosphate from ammonia and bicarbonate, is also upregulated, and could maintain the pyrimidine pool and DNA synthesis, as observed in cancer cells.[39]

To confirm that key enzymes of arginine metabolism involved in the synthesis of polyamines and phosphocreatine are upregulated in *NRF2*$^{-/-}$ cells, we performed qRT-PCR and NRF2 rescue experiments. Figure 4E shows that *ARG2*, *GATM*, *CPS1*, and *AGMAT* are significantly upregulated in *NRF2*$^{-/-}$ cells, which is in excellent agreement with the RNA-seq data. Their expression drops to the level of WT cells when *NRF2* is re-expressed. While cytosolic CKB does not change in NRF2$^{-/-}$ cells (Figure S5A), the mitochondrial isoenzymes *CKM1A* and *CKM1B* are strongly downregulated (Figure 4F). Finally, *GLUL* is strongly expressed in *NRF2*$^{-/-}$ cells as it converts glutamate to glutamine, which is essential for the synthesis of purine and pyrimidine nucleotides (Figure 4G).

An insight into the creatine pathway was gained from metabolomic experiments which showed a sharp increase in phosphocreatine in *NRF2*-deficient cells compared to WT cells: from ~0.05 to ~1.5 nmol/10^7 cells (Figure 5A). From the levels of arginine and guanidinoacetate, we concluded that ~37% of the arginine in *NRF2*$^{-/-}$ cells are directed into the creatine pathway. The activity of creatine kinase is particularly high in NRF2$^{-/-}$, about 3 orders of magnitude higher than in WT cells (Figure 5B). Cytoplasmic CKB plays a key role in the energy homeostasis of the cell by reversibly catalyzing the transfer of phosphate between ATP and creatine. The energetic role of CKB in NRF2$^{-/-}$ cells was demonstrated by silencing CKB with esiRNAs (endoribonuclease-prepared siRNA) and measuring ATP production (Figures 5C and 5D). As expected, this treatment had no effect in WT cells, while it decreased ATP production in *NRF2*$^{-/-}$ cells by 40%, indicating a crucial role of the creatine pathway in these non-glycolytic cells. As shown in Figure 4C, arginine can feed also the synthesis of polyamines either via

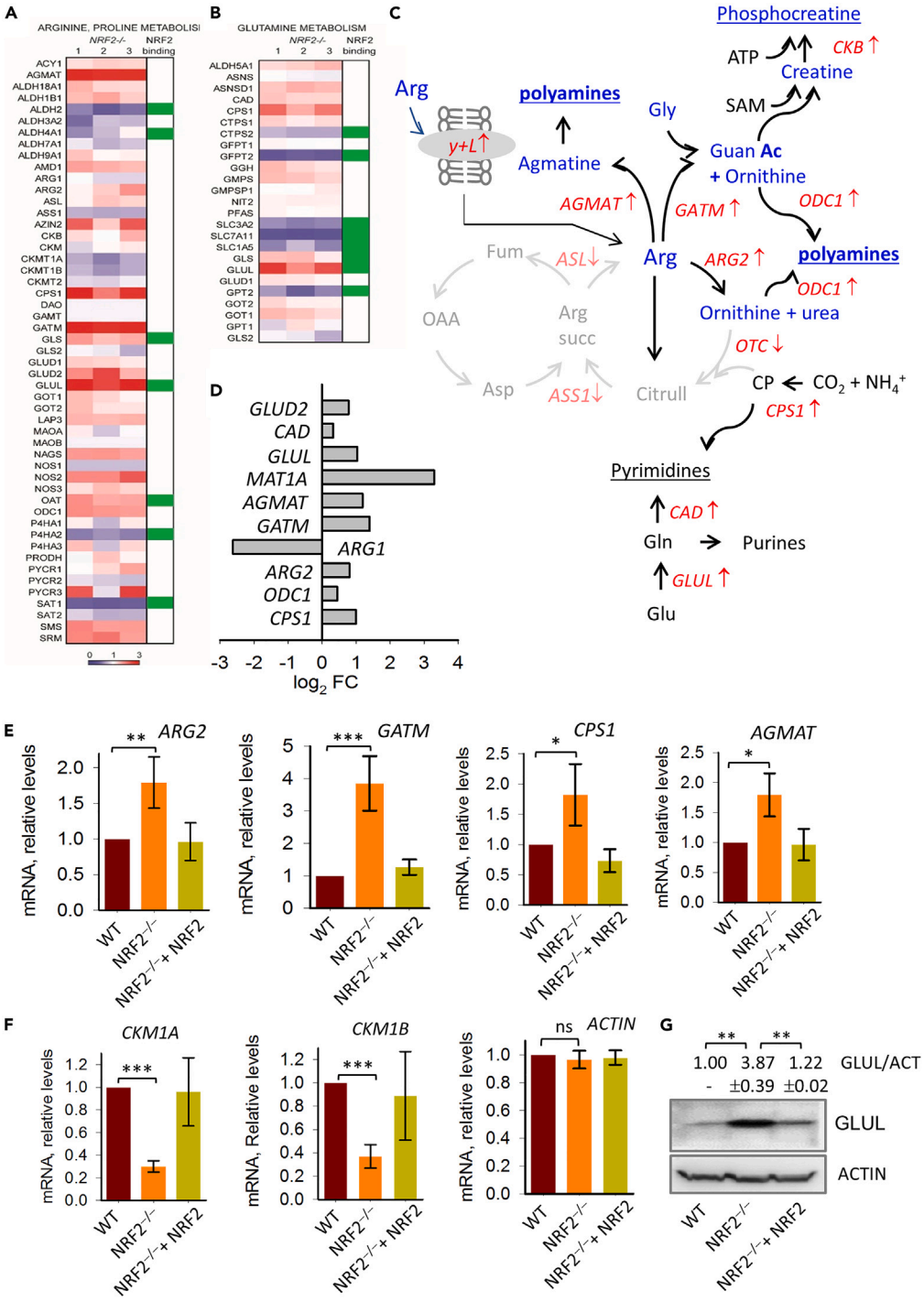

Figure 4. NRF2 depletion leads to the activation of alternative energy supply pathways

(A and B) Heatmaps showing DEG clusters involved in arginine/proline and glutamine metabolism.

(C) Metabolic network showing the fate of arginine in Panc-1 cells lacking the $KRAS^{G12D}$-NRF2 axis. The cells respond to NRF2 deletion by channeling arginine toward creatine, polyamines and nitric oxide metabolism. Enzymes involved in the metabolic pathways are shown, ↓ = downregulated, ↑ = upregulated.

(D) Log_2 (fold change) of some key DEGs ($p < 0.05$) involved in arginine metabolism.

(E and F) Expression level of some key enzymes determined by qRT-PCR. As a control, we re-expressed NRF2 in *NRF2*$^{-/-}$ cells. The enzymes CKM1A and CKM1B are ckb isozymes localized in the mitochondria.

(G) Expression of GLUL was measured by western blot. Data represent the mean ± s.d. of at least 3 independent experiments: *$p \leq 0.05$; **$p \leq 0.01$; ***$p \leq 0.001$ by Student's *t* test.

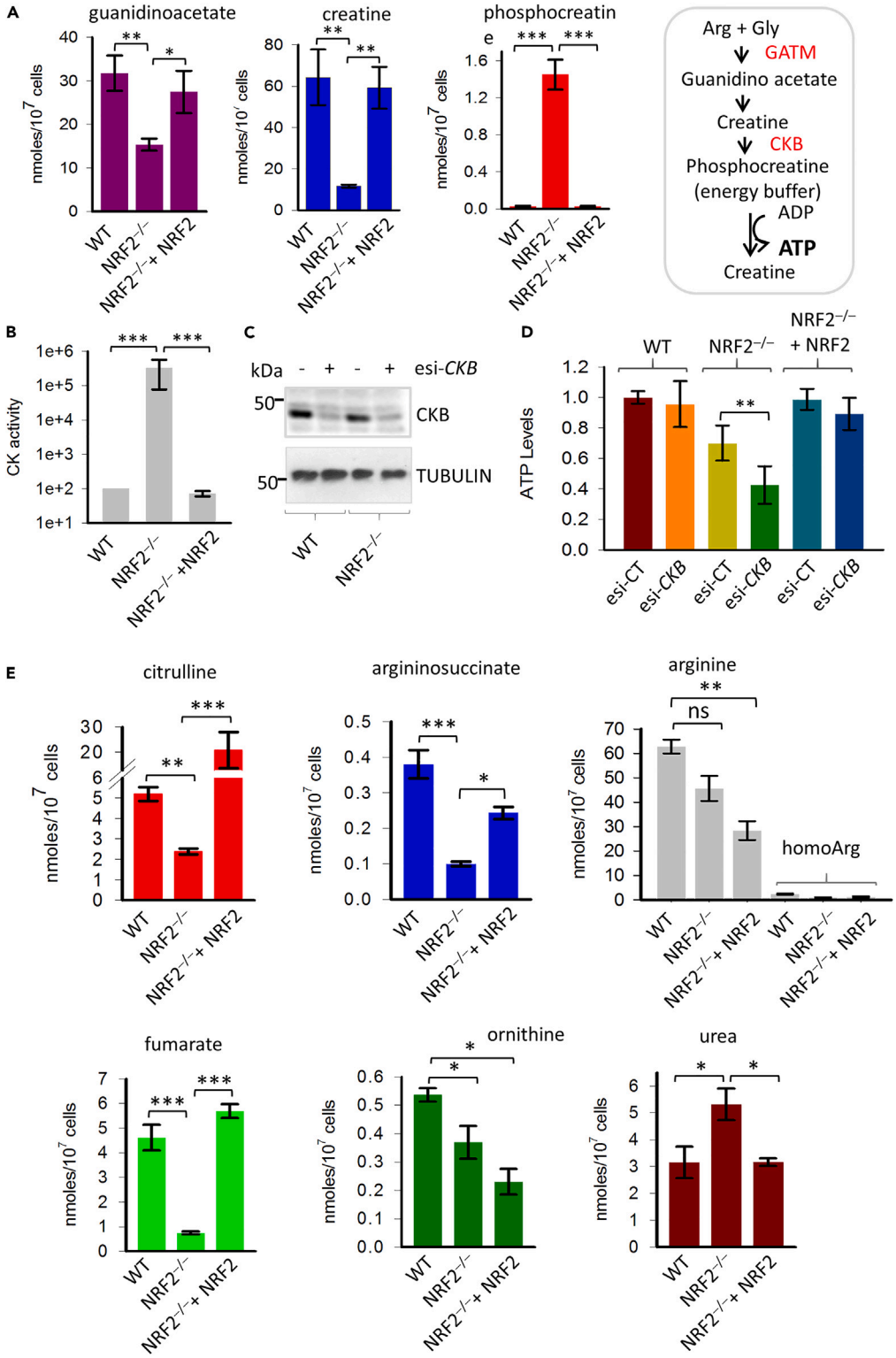

Figure 5. Arginine catabolism meets the energy needs of *NRF2*$^{-/-}$ cells

(A) Creatine biosynthesis intermediates in WT, *NRF2*$^{-/-}$ and *NRF2*$^{-/-}$ added with NRF2 cells.

(B) Creatine kinase enzyme activity in WT, *NRF2*$^{-/-}$ and *NRF2*$^{-/-}$ added with NRF2 cells.

Figure 5. *Continued*

(C) Western blot showing suppression of CKB with esiRNAs against CKB.

(D) ATP levels in WT, *NRF2*$^{-/-}$ and *NRF2*$^{-/-}$ cells re-expressing NRF2. Suppression of CKB leads to a strong decrease in ATP levels.

(E) Urea cycle intermediates in WT, *NRF2*$^{-/-}$ and *NRF2*$^{-/-}$ re-expressing NRF2. Data represent the mean ± s.d. of 5 independent experiments: *p ≤ 0.05; **p ≤ 0.01; ***p ≤ 0.001 by Student's *t* test (paired comparison) or Dunn's multiple comparison test.

AGMAT or via ARG2 and *ornithine decarboxylase* (ODC1). We found increased levels of polyamines in *NRF2*$^{-/-}$ cells (Figure S5B). Polyamines have important cellular functions and promote cancer progression.[36,40] Elevated polyamine and ODC1 levels have been reported to contribute to pancreatic carcinogenesis.[41,42] In addition, a recent study has shown that AGMAT promotes cell proliferation and metastasis in colorectal and pancreatic cancer.[43] qRT-PCR and RNA-seq showed that *AGMAT* is expressed ∼ 2-fold more in *NRF2*$^{-/-}$ cells than in WT cells (Figure 4E). The low level of fumarate and argininosuccinate in *NRF2*$^{-/-}$ cells (Figure 5E) correlates with low expression of *ASS1* and *ASL* in these cells. Since arginine and ornithine feed the creatine and polyamine pathways, their content is lower in NRF2$^{-/-}$ cells than in WT. In fact, the consumption of arginine in NRF2$^{-/-}$ cells is 2-fold higher than in WT cells (Figure S5C). We were surprised that arginine levels were not restored in *NRF2-rescue* cells. This could be due to the fact that the y+L transporter and the urea cycle respond to *NRF2* on a timescale higher than that of the rescue experiment. The higher level of urea in *NRF2*$^{-/-}$ cells is due to the fact that arginine feeds the polyamine pathway. Overall, transcriptome, metabolome and *NRF2* rescue experiments show that inhibition of the *KRAS*^{G12D}-*NRF2* axis in Panc-1 cells leads to profound metabolic rewiring that deactivates glycolysis and promotes the use of amino acids, particularly arginine, for survival and proliferation. In addition, down-regulation of *ASS1* and *OTC* in *NRF2*$^{-/-}$ cells arrests the synthesis of arginine. This auxotrophic effect for arginine makes cells dependent on arginine from the extracellular environment: a vulnerability that may be relevant for the development of new therapeutic strategies.

Amino acid catabolism is a necessary ATP source in Panc-1 *NRF2*$^{-/-}$ cells

To further investigate the metabolic reprogramming resulting from the suppression of the *KRAS-NRF2* axis, we tested how WT and *NRF2*$^{-/-}$ cells respond to glucose, glutamine and arginine restrictions. In both cell lines, glutamine starvation dramatically drops cell viability to ∼20% of the value observed in DMEM (Figure 6A), consistent with a strong glutamine dependence of PDAC cells as previously observed[19,44,45]. The exposure of WT and *NRF2*$^{-/-}$ cells to low glucose (LG, 5.5 mM) or 2-deoxyglucose (2DG, 25 mM), a molecule that inhibits glycolysis, induced a stronger reduction of cell viability of WT cells (∼45% of DMEM) compared to *NRF2*$^{-/-}$ cells (∼70% of DMEM), as the latter are less glucose-dependent than the former. When glutamine was removed from LG medium, cell viability further dropped, consistent with the critical role played by glutamine in both WT and *NRF2*$^{-/-}$ cells.[19,27] We then measured ATP production (pmoles ATP/cell) under DMEM (25 mM glucose) and LG (5.5 mM glucose) conditions (Figure 6B). As expected, WT cells show a dramatic difference in ATP production between the two glucose conditions (>70%), which is due to their glycolic nature. In DMEM, the ATP content in *NRF2*$^{-/-}$ clones KO-134 and KO-16 is lower than in WT cells. In contrast, the KO clones in LG have a significantly higher ATP content than WT cells because they switch to aerobic metabolism. Together, the data demonstrate that *NRF2*$^{-/-}$ cells are less glucose dependent than WT cells, while both types of cells show a strong dependence on glutamine. This is in keeping with the increase of ECAR and the sensitivity to sodium oxamate, an LDHA inhibitor, of WT and *NRF2*$^{-/-}$ + *NRF2* cells compared to *NRF2*$^{-/-}$ cells (Figure S6A).

We also investigated the contribution of amino acids (Gln, Arg and non-essential amino acids (NEAA)) to ATP production (Figure S6B). We found that arginine and NEAA are not critical for ATP production in WT cells under LG conditions. In contrast, *NRF2*$^{-/-}$ cells lacking the *KRAS*^{G12D}-*NRF2* axis showed a decrease in ATP production in LG medium without arginine or glutamine. Taken together, the data suggest that WT cells are glycolytic, while *NRF2*$^{-/-}$ cells are not and show dependence on glutamine and arginine in accordance with metabolomic data. As we previously concluded that *NRF2*$^{-/-}$ cells are auxotrophic for arginine, we measured their capacity of colony formation under DMEM and LG conditions, with and without arginine (Figure 6C). *NRF2*$^{-/-}$ cells showed a clonogenic growth in DMEM ∼20% lower than that of WT cells. As a control, a NRF2-rescue experiment was performed. In contrast, the number of colonies dropped dramatically by ∼ 80% in LG medium without arginine, in all three cell lines. Remarkably, when arginine was supplemented, colony formation of *NRF2*$^{-/-}$ cells significantly increased from 10 to 50%, compared to colony formation in DMEM. On the contrary, WT and NRF2-rescue cells did not increase the number of colonies. Moreover, the percentage of colonies formed by WT and *NRF2*$^{-/-}$ Panc-1 cells in arginine-free DMEM medium was drastically lower than in arginine-containing DMEM medium (Figure S6C).

Interestingly, the data demonstrate that a metabolic circuit is activated in *NRF2*$^{-/-}$ Panc-1 cells that is highly dependent on arginine to ensure malignancy, survival and growth.

The independence from glucose of *NRF2*$^{-/-}$ cells is even more evident by growing them as 3D spheroids in Matrigel (Figure 6D). *NRF2*$^{-/-}$ cells formed smaller spheroids with respect to WT cells in DMEM, but not in LG medium (Figure 6E). Similarly, while in DMEM (high-glucose) the rate of *NRF2*$^{-/-}$ spheroids displaying invasive properties was half than that of WT, in LG conditions it increases nearly 2-fold (Figure 6F).

An important sensor of cellular energy is AMPK, which is activated by phosphorylation at threonine 172 when intracellular ATP is low. The net effect of pAMPK is stimulation of glucose uptake/β-oxidation and inhibition of anabolism.[46] We measured the levels of AMPK and pAMPK in WT and *NRF2*$^{-/-}$ 3D spheroids under DMEM or low-glucose conditions (Figures S7A and S7B). Glycolytic WT cells showed a 9-fold increase of pAMPK in LG, attesting that the primary source of ATP in these cells is glucose. In contrast, *NRF2*$^{-/-}$ cells showed a lower increase of pAMPK (∼4-fold) in LG, consistent with the fact they are less dependent on glucose as energy source. Taken together, these results demonstrate that the malignant and invasive properties retained by NRF2-deficient cells are independent from glucose metabolism, but relay on arginine catabolism.

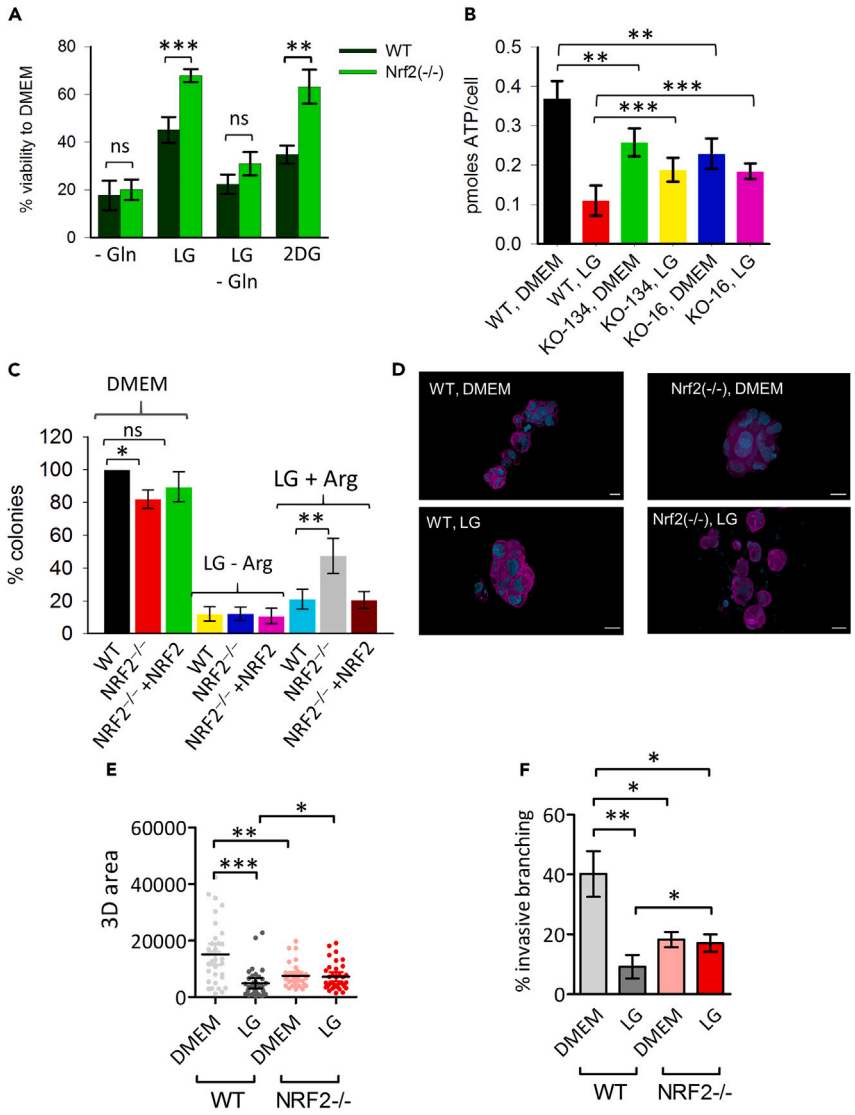

Figure 6. Depletion of NRF2 makes Panc-1 cells addicted to amino acids, especially arginine, but less sensitive to glucose restriction

(A) % Cell viability relative to DMEM of WT, NRF2$^{-/-}$ and NRF2$^{-/-}$ +NRF2 Panc-1 cells in medium without glutamine (-Gln), low glucose (LG), LG without glutamine and 2-deoxyglucose (2DG).

(B) Amount of ATP (pmol ATP/cell) in WT and NRF2$^{-/-}$ cells, clone KO-134 and KO-16 cells in DMEM (high glucose) and LG.

(C) % colonies in WT, NRF2$^{-/-}$ and NRF2$^{-/-}$ re-expressing NRF2 cells cultured in DMEM, LG without arginine and LG with added arginine.

(D) Confocal microscopy images of WT and NRF2$^{-/-}$ spheroids embedded in Matrigel and cultured in DMEM (high glucose) or LG for 4 days. Length scale bar = 10μm.

(E and F) Growth of WT, NRF2$^{-/-}$ and NRF2$^{-/-}$ +NRF2 spheroids in DMEM or LG. The percentage of WT and NRF2$^{-/-}$ spheroids showing invasive/branching structures when grown in DMEM and LG for 4 days; Data represent the mean ± s.d. of at least 3 independent experiments: *p ≤ 0.05; **p ≤ 0.01; ***p ≤ 0.001 by Student's *t* test (paired comparison) or Dunn multiple comparisons test.

Effect of cyclocreatine on PDAC growth and its design of combination therapies

To investigate the effects of the phosphocreatine pathway on cell growth, we used cyclocreatine and homoarginine as competitive inhibitors of CKB and GATM/AGMAT/ARG2, respectively. Figures 7A and 7B shows the ability of WT and *NRF2*$^{-/-}$ cells to form 3D spheroids in the presence and absence of cyclocreatine (CCr). The results show that: (1) the 3D spheroid invasion rate of *NRF2*$^{-/-}$ Panc-1 cells is ~30% lower than that of WT cells, consistent with the growth observed in 2D cell culture reported in Figure S3C; (2) the 3D spheroid invasion rate of *NRF2*$^{-/-}$ Panc-1 cells decreases by ~70% in the presence of CCr, while the invasion rate of WT cells decreases by ~25%. These data suggest that the phosphocreatine pathway is energetically central to the growth of *NRF2*$^{-/-}$ Panc-1 cells, whereas this is not the case for WT cells. Indeed, CCr (5 mM) and homoarginine (5 mM) reduce ATP levels in *NRF2*$^{-/-}$ cells by ~50 and 65%, respectively. In contrast, the

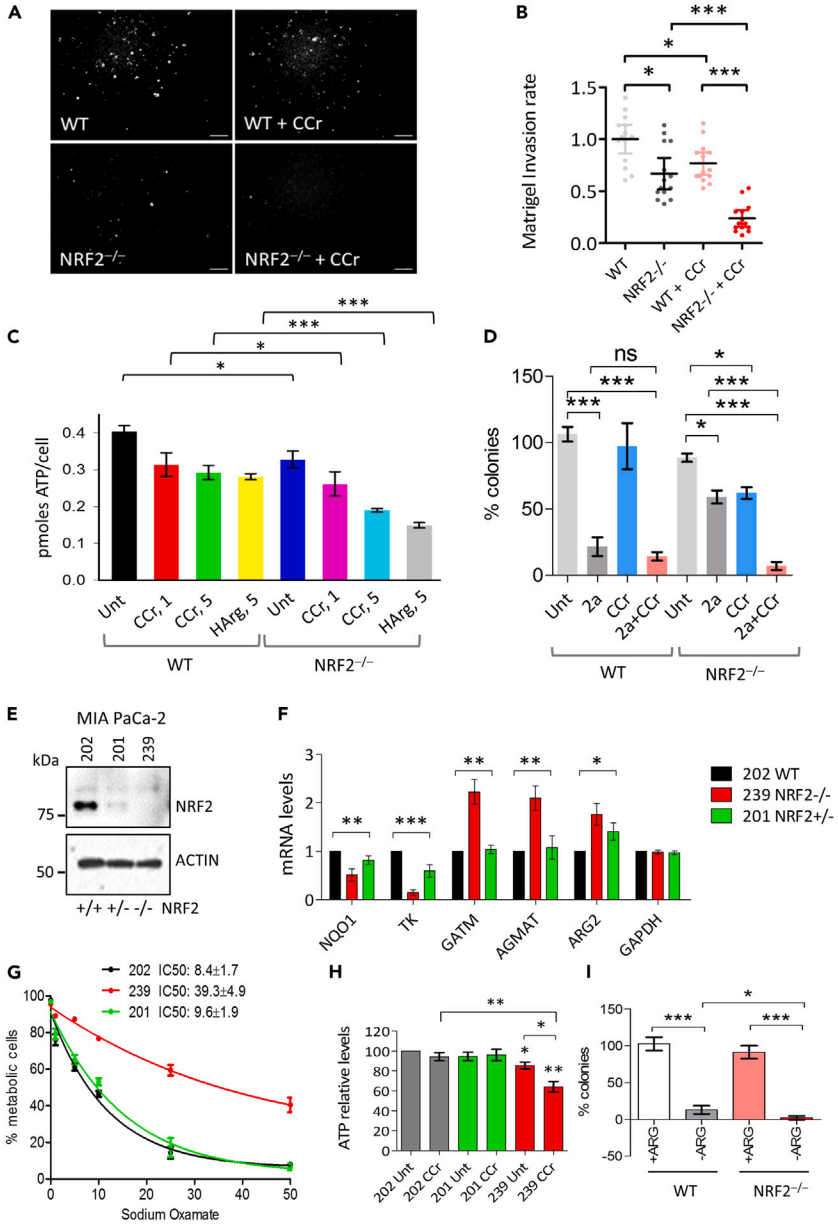

Figure 7. Effect of cyclocreatine on PDAC growth

(A) Epifluorescence microscopy images of Hoechst + WT and *NRF2*$^{-/-}$ cells invading a 3D matrix after exposure to 20% FBS as chemoattractant for 16 h in the presence or absence of cyclocreatine.

(B) Matrigel invasion rate in the absence and presence of CCr of 3 × 10^5 WT and NRF2$^{-/-}$ cells grown in 0.1% FBS/DMEM or 0.1% FBS/DMEM + 5mM CCr resuspended and seeded in 24mm Transwell with 8.0 μm pore polycarbonate membrane coated with Matrigel solution. Matrix invasion into the lower chamber containing 20% FBS/DMEM was measured 16 h after seeding by staining the invading cells with DAPI. For each experiment, the invasion rate of 5 randomly selected high-power fields was evaluated.

(C) ATP production (pmol ATP/cell) in WT and *NRF2*$^{-/-}$ cells treated with 1 and 5 mM cyclocreatine or 5 μM homoarginine for 48 h.

(D) Effect on colony formation of anthrathiophenedione 1.6 μM **2a** in the absence or presence of 5 μM cyclocreatine (CCr) by WT and *NRF2*$^{-/-}$ cells.

(E) Immunoblot evaluation of NRF2 levels in WT (clone 202), *NRF2*$^{+/-}$ (clone 201) and *NRF2*$^{-/-}$ (clone 239) MIA PaCa-2 cells.

(F) mRNA expression level of the indicated genes in MIA PaCa-2 clones compared to WT cells.

(G) MIA PaCa-2 clones were treated with the indicated mM concentrations of sodium oxamate for 60 h and subjected to a resazurin/resorufin assay. IC50 was calculated using an unadjusted third-degree polynomial regression curve.

(H) histogram showing the ATP levels of the indicated cells treated or not with 5 mM CCr for 72 h. Data refer to untreated WT cells.

(I) Percentage of colony formation of WT and *NRF2*$^{-/-}$ MIA-PaCa-2 cells in the presence and absence of arginine. Data represent the mean ± s.d. of at least 3 independent experiments: *p ≤ 0.05; **p ≤ 0.01; ***p ≤ 0.001 by Student's *t* test (paired comparison) or Dunn multiple comparison test.

two inhibitors reduced ATP in WT cells by only 25%, indicating that the creatine pathway is not critical in these cells (Figure 7C). Furthermore, knockout of *CKB* resulted in a significant decrease in proliferation and increase in cell doubling time in *NRF2*$^{-/-}$ cells, but not in WT cells (Figures S7C and S7D). We also examined whether CCr sensitizes PDAC cells to anticancer drugs in combination therapy. We used anthrathiophenedione **2a**, which inhibits the expression of *KRAS*,[47] as an anticancer drug for PDAC. Figure 7D shows that 1.6 μM **2a**, which suppresses the *KRAS* gene and thus the *KRAS*^{G12D}-*NRF2* axis, reduced the ability to form colonies in WT cells by ~75%. When the cells were treated with **2a** and CCr together, stronger suppression of colony formation was observed (from ~75 to 90%). The CCr effect was more pronounced in *NRF2*$^{-/-}$ cells (from ~60 to 95%), as they rely heavily on the creatine pathway. The synergistic effect of the combination of **2a** and CCr was evaluated according to Bliss synergy score and found to be 0.55 for WT Panc-1 cells and 7.7 for *NRF2*$^{-/-}$ Panc-1 cells (Figure S7E).[48]

Next, we decided to validate our findings in a second cell model and chose PDAC MIA PaCa-2 cells carrying the biallelic mutation on *KRAS* (*KRAS*^{G12C}) and exhibiting a highly glycolytic metabolism.[49] We obtained a *NRF2*$^{-/-}$ biallelic knockout clone (KO-239) and a heterozygous *NRF2*$^{+/-}$ clone (KO-201) (Figure 7E) by CRISPR-Cas 9 (Figure S8A). In addition, a *NRF2*$^{+/+}$ clone (202) was used as wild-type clone. Consistent with observations in Panc-1 cells, knockout of *NRF2* in MIA PaCa-2 resulted in transcriptional repression of *NQO1* and *TKT* and increased expression of *ARG2*, *AGMAT* and *GATM*, whereas deletion of an *NRF2* allele had minimal effect on transcription of these genes (Figure 7F). These results suggest that suppression of *NRF2* in MIA PaCa-2 cells causes an arginine-based metabolic shift similar to that observed in Panc-1. To confirm this behavior, we exposed the three MIA PaCa-2 clones to increasing concentrations of the LDHA inhibitor sodium oxamate for 60 h and measured the metabolic activity of the cells using the resazurin-resorufin conversion assay (Figure 7G). *NRF2*$^{+/+}$ and *NRF2*$^{+/-}$ MIA PaCa-2 cells were very sensitive to sodium oxamate treatment (IC_{50} < 10 mM), while *NRF2*$^{-/-}$ MIA PaCa-2 cells were resistant to it (IC_{50} ~ 40 mM), in keeping with the fact that they are not dependent on aerobic glycolysis. The treatment with 5 mM CCr showed a significant effect on ATP production only in *NRF2*$^{-/-}$ KO -239 (Figure 7H). Importantly, *NRF2*$^{-/-}$ MIA PaCa-2 cells, like Panc-1 cells, produce more polyamines (Figure S5B) and consume more arginine (Figure S5C) than WT cells and are very sensitive to arginine deficiency (Figure 7I).

Finally, the inhibition of NRF2 in Panc-1 and MIA PaCa-2 cells by ML385 enhances arginine auxotrophy, as the deprivation of exogenous arginine in the presence of ML385 almost completely blocks colony formation in both cell lines (Figures S8B and S8C). Taken together, our data show that suppression of *NRF2* in PDAC cells activates a collateral survival mechanism that makes the cells less dependent on aerobic glycolysis and therefore less susceptible to inhibition by *KRAS*, but dependent on arginine metabolism and therefore susceptible to blockade of the creatine phosphagen system.

Suppression of *KRAS-NRF2* axis and activation of collateral metabolic routes in PDAC patients and patient-derived organoids displaying acquired resistance to neoadjuvant FOLFIRINOX treatment

Resistance to neoadjuvant combination therapies, which is responsible for the poor outcome of patients with PDAC, remains a major challenge in oncology.[50,51] We asked whether the inhibition of the *KRAS*^{G12D}-*NRF2* axis and activation of arginine-creatine metabolism is also induced in patients receiving neoadjuvant treatment with FOLFIRINOX. To address this question, we re-analyzed RNA-seq data from two PDAC patient-derived organoids (PDOs): a pre-treatment PDO (ID188) and a post-treatment PDO (ID211) obtained from surgical resection specimens after FOLFIRINOX treatment (GSE193389).[51] GSEA analysis revealed significant overlap between genes repressed in ID211 versus ID188 and genes downregulated in our *NRF2*$^{-/-}$ PDAC cells. Interestingly, the genes that are more repressed in ID211 and contribute to core enrichment belong to the KEGG categories "glycolysis" and "genes upregulated by oncogenic KRAS" (Figure 8A; Table S2). Reciprocal analysis confirmed that the signature downregulated in our *NRF2*$^{-/-}$ Panc-1 cells is indeed repressed in ID211, further highlighting that both KRAS and NRF2 signaling are knocked down in ID211 (Figure 8B). These results were confirmed by an independent dataset (GSE169321).[52] Here, the transcriptome of five PDOs obtained from resected tumor biopsies from patients who had received eight cycles of neoadjuvant FOLFIRINOX chemotherapy prior to surgery was compared with five treatment-naïve samples. Genes that were repressed in FOLFIRINOX samples were also significantly repressed in our *NRF2*$^{-/-}$ Panc-1 cells (Figure 8C), indicating an alteration of PDAC metabolism and impairment of aerobic glycolysis in PDOs exposed to FOLFIRINOX treatment (Figure 8C). We then identified a signature of seven genes encoding key enzymes of arginine metabolism that we found to be directly regulated by NRF2 (Figure 8D). We defined this signature as the "NRF2-regulated arginine-auxotrophic signature". Importantly, this signature was significantly upregulated in ID211 compared to ID188 (Figure 8E). Finally, PDAC patients who were found to be characterized by the upregulation (*Z* score >3) of at least one gene belonging to this signature were characterized by higher genome instability (expressed as the proportion of the genome altered, F.G.A.) and a lower hypoxia score (Figure 8F). Consistent with our data, the signature of six core NRF2-regulated genes (*G6PD, GSTM4, NQO1, GCLM, HMOX1, PRDX1*) was found significantly suppressed in PDAC patients characterized by upregulation of the "NRF2-regulated arginine-auxotrophic signature", while the suppression of *LDHA* and the lower hypoxia index may indicate a shutdown of aerobic glycolytic mechanisms (Figure 8G). We then divided the cohort of PDAC patients into two groups based on the expression of the "NRF2-regulated arginine-auxotrophic signature". Remarkably, patients with higher expression of the signature (above the median) had a worse prognosis (Figure 8H), despite having no obvious genetic alterations, compared to the group with lower expression of the signature. Overall, these data suggest that suppression of the *KRAS-NRF2* axis and activation of collateral arginine-based metabolic pathways can be observed in PDAC patients undergoing neoadjuvant FOLFIRINOX therapy and could be used to overcome acquired resistance.

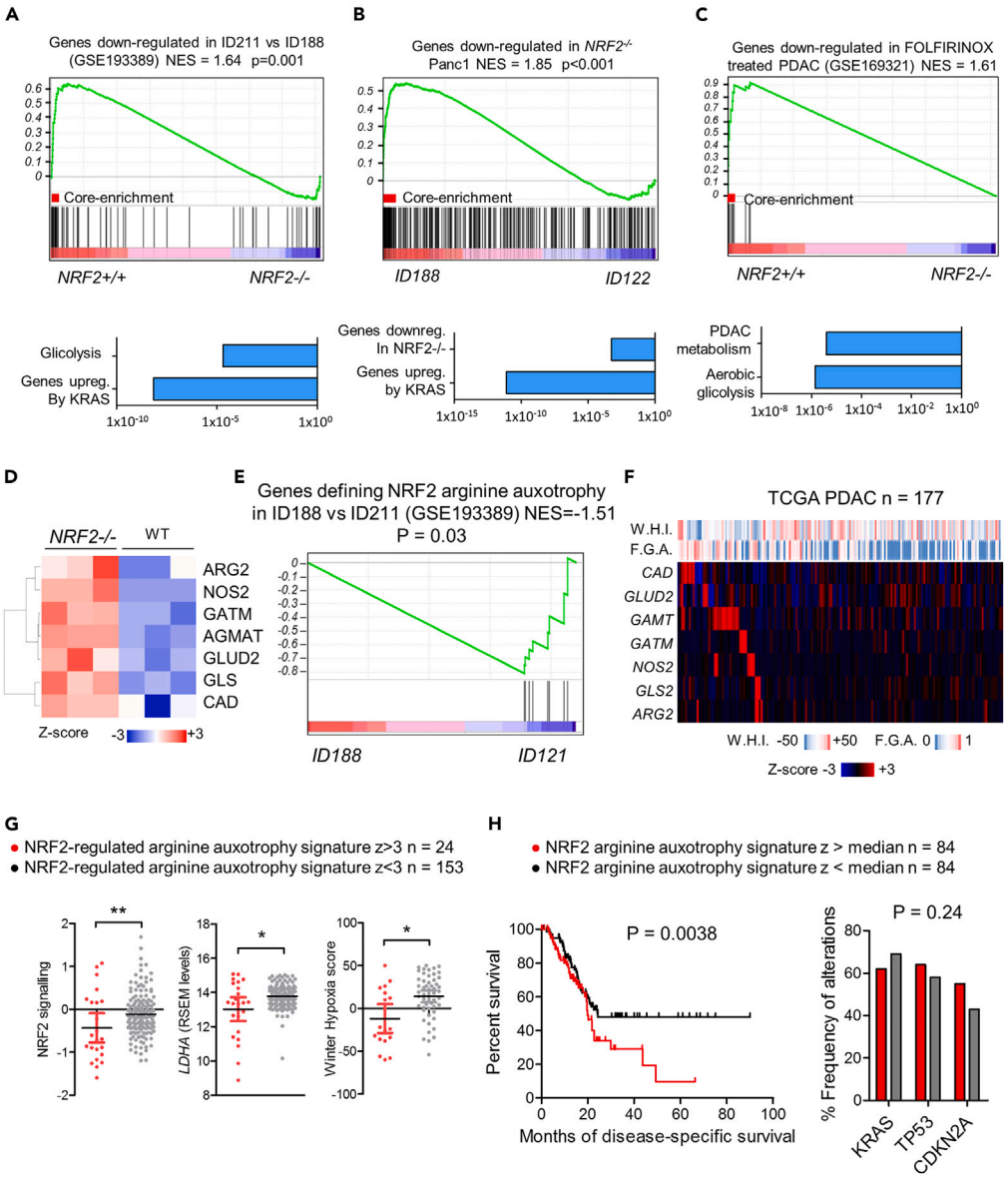

Figure 8. The KRAS/NRF2 axis is switched off and arginine metabolism is switched on in PDAC developing resistance to FOLFIRINOX

(A) GSEA plot using as geneset genes downregulated in ID211 compared to ID188 (Table S2) and our RNA-seq dataset. Functional enrichment was performed on core-enriched genes and expressed as FDR (False Discovery Rate).

(B) GSEA plot obtained by using as geneset the top 500 genes downregulated in *NRF2*$^{-/-}$ Panc-1 cells and GSE193389 as the dataset. Functional enrichment was performed on the core-enriched genes and expressed as FDR.

(C) GSEA plot obtained by using as geneset genes downregulated in PDOs obtained from FOLFIRINOX-treated patients and our RNA-seq dataset. Functional enrichment was performed on the core-enriched genes and expressed as FDR.

(D) Heatmap of NRF2-regulated arginine-auxotrophic genes.

(E) GSEA plot obtained by using as geneset the "NRF2-regulated arginine-auxotrophic signature" and GSE193389 as the dataset.

(F) Heatmap of 177 TCGA-PDAC patients ranked accordingly to the expression of the seven indicated genes representing the "NRF2-regulated arginine-auxotrophic signature". For each sample, the Winter hypoxia index (W.H.I.) and the fraction of the genome altered (F.G.A.) are indicated above the heatmap.

(G) Dot plots showing the expression levels, expressed as z-scores, of NRF2 signaling (*G6PD, GSTM4, NQO1, GCLM, HMOX1, PRDX1*), LDHA and Winter Hypoxia score in patients with increased expression of the "NRF2-regulated arginine auxotrophic signature" (z > 3, indicated in red) compared to other patients (indicated in gray).

(H) Left, Kaplan-Meier survival analysis in 168 TCGA-PDAC patients characterized by high (above the median, in red) or low (below the median, in blue) expression of the "NRF2-regulated arginine auxotrophic signature"; right: histogram representing the frequency of genetic alterations of the indicated oncogenes and tumor suppressors in the two identified patient groups.

DISCUSSION

In this study we report that redox homeostasis and metabolic reprogramming are under the control of the *KRAS-NRF2* axis in pancreatic cancer cells. To investigate the effects of the *KRAS-NRF2* axis on pancreatic cancer cell metabolism, we knocked down *NRF2* in Panc-1 cells using CRISPR-Cas9. RNA-seq analysis showed that knocking down *NRF2* resulted in down-regulation of 666 genes and up-regulation of 1888 genes. Functional enrichment analysis of DEGs showed strong impairment of sugar catabolism (glycolysis and PPP) and glutathione biosynthesis. Our results are consistent with those of Fu et al.,[27] who grouped gene microarray data from 53 cases of human ESCC (GEO23400) into *NRF2*-high (n = 17) and NRF2-low (n = 36). When comparing gene expression between the two groups, they found that metabolic genes involved in glycolysis, PPP and GSH were overexpressed in high NRF2 ESCC. Furthermore, De Pinho et al.[9] reported that $KRAS^{G12D}$ in PDAC strongly controls glycolysis and PPP at the transcriptional level. Since $KRAS^{G12D}$ controls *NRF2* expression, metabolic reprogramming in PDAC is most likely controlled by the *KRAS-NRF2* axis. Studies using genetically engineered mouse models have also shown the crucial role of NRF2 in cancer and its cooperation with KRAS in promoting tumorigenesis.[11,53–55]

It is generally accepted that a promising therapeutic approach for PDAC is based on suppression of the oncogenic *KRAS* or inhibition of the encoded protein by small molecules.[15,21,56,57] This should turn off the *KRAS-NRF2* axis and promote a metabolic reprogramming of arginine metabolism. PDAC cells become arginine-auxotrophic and depend on exogenous arginine from the extracellular environment. Under these metabolic conditions, exogenous arginine is used for the synthesis of phosphocreatine and polyamines: two molecules that support cell growth. Indeed, it has been reported that genetic silencing of a key enzyme of *de novo* synthesis of creatine such as GATM with shRNA leads to a decrease in cell proliferation and an increase in apoptosis in FLT3- ITD -mutated cell lines.[58] In addition, a recent study has shown that the creatine kinase signaling pathway can metabolically support the migration and invasion of pancreatic cancer cells.[17] The authors found that although cancer cells rely on glucose consumption and aerobic glycolysis, they exhibit efficient metabolic plasticity that is controlled by the mechanical properties of the microenvironment, such as the stiffness of the extracellular matrix (ECM). In particular, the ECM mechanics were found to control arginine metabolism by diverting arginine from UC to creatine synthesis. This system supplies cells with energy when their demand is increased[17]. A key gene of the phosphocreatine pathway is *CKB*, whose protein catalyzes the reversible phosphorylation of creatine to phosphocreatine: a phosphagen compound that be used to generate cellular energy by converting ADP to ATP. The phosphocreatine energy system supports pancreatic cancer cells when they are under metabolic stress due to loss of the *KRAS-NRF2* axis, which restricts the use of glucose. GSEA shows that in *NRF2*-deficient cells, KRAS signaling is lost, while MYC signaling is upregulated probably to maintain malignancy. When aerobic glycolysis flux is reduced, PDAC cells shift their metabolism from glucose to amino acids (glutamine and arginine). Unbiased functional enrichment analyses showed that arginine metabolism plays a role in cell adaptation to metabolic stress. As the repression of the *KRAS-NRF2* axis increases arginine dependence in pancreatic cancer cells, the inhibition of the creatine pathway by CCr or homoarginine is an interesting therapeutic approach for PDAC. Indeed, we have shown that both CCr and homoarginine significantly reduce the ability of WT and $NRF2^{-/-}$ cells to form 3D spheroids in Matrigel matrix 3D plates. The metabolic reprogramming induced by the suppression of the *KRAS-NRF2* axis was observed not only in Panc-1 but also in MIA PaCa-2 cells, suggesting the transversality of our observation. It is worth mentioning that the opposite conditions, i.e., *NRF2* activation in *KRAS*-driven pancreatic cancers, rewires metabolism to elevate glutamine consumption and create glutamine "addiction".[19,44,45]

Remarkably, the transcriptome of PDAC PDOs obtained from surviving cancer biopsies of patients treated with FOLFIRINOX overlapped significantly with that of $NRF2^{-/-}$ PDAC cells. In addition, our bioinformatic analysis revealed that the surviving FOLFIRINOX PDAC clones turn off the *KRAS-NRF2* axis and activate arginine metabolism. Finally, our study also suggests that monotherapies based on inhibition of *KRAS* are likely to be less efficient than combination therapies targeting both the *KRAS-NRF2* axis and the arginine/creatine metabolic pathway.

Limitations of the study

The 5-year survival rate of PDAC patients is 12% as the disease develops resistance to conventional chemotherapy. Due to these poor therapeutic outcomes, new therapeutic strategies are urgently needed. Our work shows that inactivation of the $KRAS^{G12D}$-*NRF2* axis leads to a decrease in glycolysis, PPP and glutathione cycling and a simultaneous activation of arginine metabolism, which feeds the synthesis of phosphocreatine. This high-energy storage compound constitutes a critical energy buffer to support proliferation. This means that combination therapies targeting both *KRAS* and creatine pathway are expected to be more effective than monotherapies. Our study has been carried out in 2D and 3D cell models and not in genetically engineered mouse models. This may represent a limit of the study.

STAR★METHODS

Detailed methods are provided in the online version of this paper and include the following:

- KEY RESOURCES TABLE
- RESOURCE AVAILABILITY
  - Lead contact
  - Materials availability
  - Data and code availability

SUPPLEMENTAL INFORMATION

Supplemental information can be found online at https://doi.org/10.1016/j.isci.2023.108566.

ACKNOWLEDGMENTS

This work was supported by AIRC (Associazione Italiana per la Ricerca sul Cancro): project number 19898 (LEX) and MFAG2020 ID 25000 (EDG). The authors thank Andrey Shchekotikhin of the Gause Institute of Moscow for providing compound **2a**.

AUTHOR CONTRIBUTIONS

L.E.X. and E.D.G.: Conceptualization, Methodology, Supervision; E.D.G., H.C., Y.C., F.A., M.C., and V.R.: Investigation, Validation; F.D.: Confocal microscopy, L.E.X. and E.D.G.: Writing – Original Draft preparation, Writing – Reviewing and Editing, L.E.X. and E.D.G.: Funding Acquisition; E.D. and E.D.G.: Bioinformatic analyses.

DECLARATION OF INTERESTS

The authors declare that they have no conflicts of interest with the content of this article.

INCLUSION AND DIVERSITY

We support inclusive, diverse, and equitable conduct of research.

Received: May 24, 2023
Revised: October 21, 2023
Accepted: November 21, 2023
Published: November 24, 2023

REFERENCES

1. Rahib, L., Wehner, M.R., Matrisian, L.M., and Nead, K.T. (2021). Estimated Projection of US Cancer Incidence and Death to 2040. JAMA Netw. Open *4*, e214708.
2. Siegel, R.L., Miller, K.D., Wagle, N.S., and Jemal, A. (2023). Cancer statistics, 2023. CA. Cancer J. Clin. *73*, 17–48.
3. Jaffee, E.M., Hruban, R.H., Canto, M., and Kern, S.E. (2002). Focus on pancreas cancer. Cancer Cell *2*, 25–28.
4. Bos, J.L. (1989). Ras oncogenes in human cancer: a review. Cancer Res. *49*, 4682–4689.
5. Hingorani, S.R., Petricoin, E.F., Maitra, A., Rajapakse, V., King, C., Jacobetz, M.A., Ross, S., Conrads, T.P., Veenstra, T.D., Hitt, B.A., et al. (2003). Preinvasive and invasive ductal pancreatic cancer and its early detection in the mouse. Cancer Cell *4*, 437–450.
6. di Magliano, M.P., and Logsdon, C.D. (2013). Roles for KRAS in pancreatic tumor development and progression. Gastroenterology *144*, 1220–1229.
7. Collins, M.A., Brisset, J.C., Zhang, Y., Bednar, F., Pierre, J., Heist, K.A., Galbán, C.J., Galbán, S., and di Magliano, M.P. (2012). Metastatic pancreatic cancer is dependent on oncogenic Kras in mice. PLoS One *7*, e49707.
8. Warburg, O. (1956). On the origin of cancer cells. Science *123*, 309–314.
9. Ying, H., Kimmelman, A.C., Lyssiotis, C.A., Hua, S., Chu, G.C., Fletcher- Sananikone, E., Locasale, J.W., Son, J., Zhang, H., Coloff, J.L., et al. (2012). Oncogenic Kras maintains pancreatic tumors through regulation of anabolic glucose metabolism. Cell *149*, 656–670.
10. Vomund, S., Schäfer, A., Parnham, M.J., Brüne, B., and von Knethen, A. (2017). Nrf2, the Master Regulator of Anti-Oxidative Responses. Int. J. Mol. Sci. *18*, 2772.
11. DeNicola, G.M., Karreth, F.A., Humpton, T.J., Gopinathan, A., Wei, C., Frese, K., Mangal, D., Yu, K.H., Yeo, C.J., Calhoun, E.S., et al. (2011). Oncogene-induced NRF2 transcription promotes ROS detoxification and tumorigenesis. Nature *475*, 106–109.
12. Ferino, A., Rapozzi, V., and Xodo, L.E. (2020). The ROS-KRAS-NRF2 axis in the control of the redox homeostasis and the intersection with survival-apoptosis pathways: Implications for photodynamic therapy. J. Photochem. Photobiol., B *202*, 111672.
13. Chio, I.I.C., Jafarnejad, S.M., Ponz-Sarvise, M., Park, Y., Rivera, K., Palm, W., Wilson, J., Sangar, V., Hao, Y., Öhlund, D., et al. (2016). NRF2 Promotes Tumor Maintenance by Modulating mRNA Translation in Pancreatic Cancer. Cell *166*, 963–976.
14. Mitsuishi, Y., Taguchi, K., Kawatani, Y., Shibata, T., Nukiwa, T., Aburatani, H.,

Yamamoto, M., and Motohashi, H. (2012). NRF2 redirects glucose and glutamine into anabolic pathways in metabolic reprogramming. Cancer Cell *22*, 66–79.
15. Di Giorgio, E., Ferino, A., Choudhary, H., Löffler, P.M.G., D'Este, F., Rapozzi, V., Tikhomirov, A., Shchekotikhin, A., Vogel, S., and Xodo, L.E. (2022). Photosensitization of pancreatic cancer cells by cationic alkyl-porphyrins in free form or engrafted into POPC liposomes: The relationship between delivery mode and mechanism of cell death. J. Photochem. Photobiol., B *231*, 112449.
16. Ellington, W.R. (2001). Evolution and physiological role of phosphagen systems. Annu. Rev. Physiol. *63*, 289–325.
17. Fenouille, N., Bassil, C.F., Ben-Sahra, I., Benajiba, L., Alexe, G., Ramos, A., Pikman, Y., Conway, A.S., Burgess, M.R., Li, Q., et al. (2017). The creatine kinase pathway is a metabolic vulnerability in EVI1-positive acute myeloid leukemia. Nat. Med. *23*, 301–313.
18. Papalazarou, V., Zhang, T., Paul, N.R., Juin, A., Cantini, M., Maddocks, O.D.K., Salmeron-Sanchez, M., and Machesky, L.M. (2020). The creatine-phosphagen system is mechanoresponsive in pancreatic adenocarcinoma and fuels invasion and metastasis. Nat. Metab. *2*, 62–80.
19. Son, J., Lyssiotis, C.A., Ying, H., Wang, X., Hua, S., Ligorio, M., Perera, R.M., Ferrone, C.R., Mullarky, E., Shyh-Chang, N., et al. (2013). Glutamine supports pancreatic cancer growth through a KRAS-regulated metabolic pathway [published correction appears in Nature. 2013;499:504]. Nature *496*, 101–105.
20. Tao, S., Wang, S., Moghaddam, S.J., Ooi, A., Chapman, E., Wong, P.K., and Zhang, D.D. (2014). Oncogenic KRAS confers chemoresistance by upregulating NRF2. Cancer Res. *74*, 7430–7441.
21. Waters, A.M., and Der, C.J. (2018). KRAS: The Critical Driver and Therapeutic Target for Pancreatic Cancer. Cold Spring Harb. Perspect. Med. *8*, a031435.
22. Shi, M.M., Kugelman, A., Iwamoto, T., Tian, L., and Forman, H.J. (1994). Quinone-induced oxidative stress elevates glutathione and induces γ-glutamylcysteine synthetase activity in rat lung epithelial L2 cells. J. Biol. Chem. *269*, 26512–26517.
23. Guyton, K.Z., Liu, Y., Gorospe, M., Xu, Q., and Holbrook, N.J. (1996). Activation of mitogen-activated protein kinase by H_2O_2. Role in cell survival following oxidant injury. J. Biol. Chem. *271*, 4138–4142.
24. McCubrey, J.A., Lahair, M.M., and Franklin, R.A. (2006). Reactive oxygen species-induced activation of the MAP kinase signaling pathways. Antioxid. Redox Signal. *8*, 1775–1789.
25. Fu, J., Xiong, Z., Huang, C., Li, J., Yang, W., Han, Y., Paiboonrungruan, C., Major, M.B., Chen, K.N., Kang, X., and Chen, X. (2019). Hyperactivity of the transcription factor NRF2 causes metabolic reprogramming in mouse esophagus. J. Biol. Chem. *294*, 327–340.
26. Lu, S.C. (2009). Regulation of glutathione synthesis. Mol. Aspects Med. *30*, 42–59.
27. Vaseva, A.V., Blake, D.R., Gilbert, T.S.K., Ng, S., Hostetter, G., Azam, S.H., Ozkan-Dagliyan, I., Gautam, P., Bryant, K.L., Pearce, K.H., et al. (2018). KRAS Suppression-Induced Degradation of MYC Is Antagonized by a MEK5-ERK5 Compensatory Mechanism. Cancer Cell *34*, 807–822.e7.
28. Spender, L.C., and Inman, G.J. (2012). Phosphoinositide 3-kinase/AKT/mTORC1/2 signaling determines sensitivity of Burkitt's lymphoma cells to BH3 mimetics. Mol. Cancer Res. *10*, 347–359.
29. Keshet, R., Szlosarek, P., Carracedo, A., and Erez, A. (2018). Rewiring urea cycle metabolism in cancer to support anabolism. Nat. Rev. Cancer *18*, 634–645.
30. Lee, M.S., Dennis, C., Naqvi, I., Dailey, L., Lorzadeh, A., Ye, G., Zaytouni, T., Adler, A., Hitchcock, D.S., Lin, L., et al. (2023). Ornithine aminotransferase supports polyamine synthesis in pancreatic cancer. Nature *616*, 339–347.
31. Long, Y., Tsai, W.B., Wang, D., Hawke, D.H., Savaraj, N., Feun, L.G., Hung, M.C., Chen, H.H.W., and Kuo, M.T. (2017). Argininosuccinate synthetase 1 (ASS1) is a common metabolic marker of chemosensitivity for targeted arginine- and glutamine-starvation therapy. Cancer Lett. *388*, 54–63.
32. Devés, R., and Boyd, C.A. (1998). Transporters for cationic amino acids in animal cells: discovery, structure, and function. Physiol. Rev. *78*, 487–545.
33. Qin, H., Sun, R., Guo, X., Fang, L., Xu, M., Teng, Y., Zhen, N., Wang, A., and Liu, J. (2023). RIOK3 promotes mTORC1 activation by facilitating SLC7A2-mediated arginine uptake in pancreatic ductal adenocarcinoma. Aging (Albany NY) *15*, 1039–1051.
34. Wallimann, T., Tokarska-Schlattner, M., and Schlattner, U. (2011). The creatine kinase system and pleiotropic effects of creatine. Amino Acids *40*, 1271–1296.
35. Ino, Y., Yamazaki-Itoh, R., Oguro, S., Shimada, K., Kosuge, T., Zavada, J., Kanai, Y., and Hiraoka, N. (2013). Arginase II expressed in cancer-associated fibroblasts indicates tissue hypoxia and predicts poor outcome in patients with pancreatic cancer. PLoS One *8*, e55146.
36. Casero, R.A., Murray Stewart, T., and Pegg, A.E. (2018). Polyamine metabolism and cancer: treatments, challenges and opportunities. Nat. Rev. Cancer *18*, 681–695.
37. Rizi, B.H., Achreja, A., and Nagrath, D. (2017). Nitric Oxide: The Forgotten Child of Tumor Metabolism. Trends Cancer *9*, 659–672.
38. Dudkowska, M., Lai, J., Gardini, G., Stachurska, A., Grzelakowska-Sztabert, B., Colombatto, S., and Manteuffel-Cymborowska, M. (2003). Agmatine modulates the in vivo biosynthesis and interconversion of polyamines and cell proliferation. Biochim. Biophys. Acta *1619*, 159–166.
39. Kim, J., Hu, Z., Cai, L., Li, K., Choi, E., Faubert, B., Bezwada, D., Rodriguez-Canales, J., Villalobos, P., Lin, Y.-F., et al. (2017). CPS1 maintains pyrimidine pools and DNA synthesis in KRAS/LKB1-mutant lung cancer cells. Nature *546*, 168–172.
40. Novita Sari, I., Setiawan, T., Seock Kim, K., Toni Wijaya, Y., Won Cho, K., and Young Kwon, H. (2021). Metabolism and function of polyamines in cancer progression. Cancer Lett. *519*, 91–104.
41. Black, O., Jr., and Chang, B.K. (1982). Ornithine decarboxylase enzyme activity in human and hamster pancreatic tumor cell lines. Cancer Lett. *17*, 87–93.
42. Subhi, A.L., Tang, B., Balsara, B.R., Altomare, D.A., Testa, J.R., Cooper, H.S., Hoffman, J.P., Meropol, N.J., and Kruger, W.D. (2004). Loss of methylthioadenosine phosphorylase and elevated ornithine decarboxylase is common in pancreatic cancer. Clin. Cancer Res. *10*, 7290–7296.
43. Zhang, Y., Cao, L., Xie, Y., Wang, C., Liu, X., Zhang, X., and Chen, J. (2022). Agmatinase facilitates the tumorigenesis of pancreatic adenocarcinoma through the TGFβ/Smad pathway. Exp. Ther. Med. *24*, 490.
44. Mukhopadhyay, S., Goswami, D., Adiseshaiah, P.P., Burgan, W., Yi, M., Guerin, T.M., Kozlov, S.V., Nissley, D.V., and McCormick, F. (2020). Undermining Glutaminolysis Bolsters Chemotherapy While NRF2 Promotes Chemoresistance in KRAS-Driven Pancreatic Cancers. Cancer Res. *80*, 1630–1643.
45. Galan-Cobo, A., Sitthideatphaiboon, P., Qu, X., Poteete, A., Pisegna, M.A., Tong, P., Chen, P.H., Boroughs, L.K., Rodriguez, M.L.M., Zhang, W., et al. (2019). LKB1 and KEAP1/NRF2 Pathways Cooperatively Promote Metabolic Reprogramming with Enhanced Glutamine Dependence in *KRAS*-Mutant Lung Adenocarcinoma. Cancer Res. *79*, 3251–3267.
46. Garcia, D., and Shaw, R.J. (2017). AMPK: Mechanisms of Cellular Energy Sensing and Restoration of Metabolic Balance. Mol. Cell *66*, 789–800.
47. Miglietta, G., Cogoi, S., Marinello, J., Capranico, G., Tikhomirov, A.S., Shchekotikhin, A., and Xodo, L.E. (2017). RNA G-Quadruplexes in Kirsten Ras (KRAS) Oncogene as Targets for Small Molecules Inhibiting Translation. J. Med. Chem. *60*, 9448–9461.
48. Demidenko, E., and Miller, T.W. (2019). Statistical determination of synergy based on Bliss definition of drugs independence. PLoS One *14*, e0224137.
49. Wang, F., Liu, H., Hu, L., Liu, Y., Duan, Y., Cui, R., and Tian, W. (2018). The Warburg effect in human pancreatic cancer cells triggers cachexia in athymic mice carrying the cancer cells. BMC Cancer *18*, 360.
50. Santana-Codina, N., Chandhoke, A.S., Yu, Q., Małachowska, B., Kuljanin, M., Gikandi, A., Stańczak, M., Gableske, S., Jedrychowski, M.P., Scott, D.A., et al. (2020). Defining and Targeting Adaptations to Oncogenic KRASG12C Inhibition Using Quantitative Temporal Proteomics. Cell Rep. *30*, 4584–4599.e4.
51. Peschke, K., Jakubowsky, H., Schäfer, A., Maurer, C., Lange, S., Orben, F., Bernad, R., Harder, F.N., Eiber, M., Öllinger, R., et al. (2022). Identification of treatment-induced vulnerabilities in pancreatic cancer patients using functional model systems. EMBO Mol. Med. *14*, e14876.
52. Farshadi, E.A., Chang, J., Sampadi, B., Doukas, M., Van 't Land, F., van der Sijde, F., Vietsch, E.E., Pothof, J., Koerkamp, B.G., and van Eijck, C.H.J. (2021). Organoids Derived from Neoadjuvant FOLFIRINOX Patients Recapitulate Therapy Resistance in Pancreatic Ductal Adenocarcinoma. Clin. Cancer Res. *27*, 6602–6612.
53. Best, S.A., Ding, S., Kersbergen, A., Dong, X., Song, J.-Y., Xie, Y., Reljic, B., Li, K., Vince, J.E., Rathi, V., et al. (2019). Distinct initiating events underpin the immune and metabolic heterogeneity of KRAS-mutant lung adenocarcinoma. Nat. Commun. *10*, 4190.

54. Singh, A., Daemen, A., Nickles, D., Jeon, S.-M., Foreman, O., Sudini, K., Gnad, F., Lajoie, S., Gour, N., Mitzner, W., et al. (2021). NRF2 Activation Promotes Aggressive Lung Cancer and Associates with Poor Clinical Outcomes. Clin. Cancer Res. *27*, 877–888.

55. Romero, R., Sayin, V.I., Davidson, S.M., Bauer, M.R., Singh, S.X., LeBoeuf, S.E., Karakousi, T.R., Ellis, D.C., Bhutkar, A., Sánchez-Rivera, F.J., et al. (2017). Keap1 loss promotes Kras-driven lung cancer and results in dependence on glutaminolysis. Nat. Med. *23*, 1362–1368.

56. Zhu, C., Guan, X., Zhang, X., Luan, X., Song, Z., Cheng, X., Zhang, W., and Qin, J.-J. (2022). Targeting KRAS mutant cancers: from druggable therapy to drug resistance. Mol. Cancer *21*, 159.

57. Tyc, K.M., Kazi, A., Ranjan, A., Wang, R., and Sebti, S.M. (2023). Novel mutant KRAS addiction signature predicts response to the combination of ERBB and MEK inhibitors in lung and pancreatic cancers. iScience *26*, 106082.

58. Zhang, Y., Newsom, K.J., Zhang, M., Kelley, J.S., and Starostik, P. (2022). GATM-Mediated Creatine Biosynthesis Enables Maintenance of FLT3-ITD-Mutant Acute Myeloid Leukemia. Mol. Cancer Res. *20*, 293–304.

59. Dobin, A., Davis, C.A., Schlesinger, F., Drenkow, J., Zaleski, C., Jha, S., Batut, P., Chaisson, M., and Gingeras, T.R. (2013). STAR: ultrafast universal RNA-seq aligner. Bioinformatics *29*, 15–21.

60. Love, M.I., Huber, W., and Anders, S. (2014). Moderated estimation of fold change and dispersion for RNA-seq data with DESeq2. Genome Biol. *15*, 550.

STAR★METHODS

KEY RESOURCES TABLE

REAGENT or RESOURCE	SOURCE	IDENTIFIER
Antibodies		
p44/42 MAPK	Cell Signalling, 137F5	AB_10695739
NRF2	Santa Cruz Biotechnology, sc-518033	AB_2892633
TKT	Santa Cruz Biotechnology, sc-390179	AB_2091939
GLUL	Santa Cruz Biotechnology, sc-74430	AB_1127501
CKB	Santa Cruz Biotechnology, sc-373686	AB_2291855
TUBULIN	Santa Cruz Biotechnology, sc-166729	AB_2288090
c-MYC	Cell Signalling, D84C12	AB_2798045
pAKT1 (Ser473)	Cell Signalling, D7F10	AB_2629283
AKT1	Cell Signalling, C73H10	AB_915788
p44/42 MAPK (Thr202/Tyr204)	Cell Signalling, D13.14.4E	AB_2728835
AMPKα	Cell Signalling, 2532	AB_490795
pAMPKα (Thr172)	Cell Signalling, 40H9	AB_10697491
GAPDH	Merck, 71.1	AB_11211543
ACTIN	Merck, A2066	AB_11212552
Anti-mouse HRP	Cell Signalling	AB_331144
Anti-rabbit HRP	Cell Signalling	AB_2099233
Chemicals, peptides, and recombinant proteins		
DMNQ	Enzo Biochem	ALX-420-027
ML-385	Tocris	6243
L-Homoarginine hydrochloride	Merck	H1007
Cyclocreatine	Santa Cruz Biotechnology	CAS 35404-50-3
Critical commercial assays		
GSH+GSSG / GSH Assay Kit	Abcam	ab239709
Free Thiol Assay Kit	Abcam	ab112158
L-Arginine Assay Kit	Merck	MAK370
Total Polyamine Assay Kit	Merck	MAK349
Deposited data		
RNA-seq data	This paper	GEO: GSE217965
Experimental models: Cell lines		
Panc-1	ATCC	CVCL_0480
MIA PaCa-2	ATCC	CVCL_0428
Phoenix Ampho	ATCC	CVCL_H716
HEK293T	ATCC	CVCL_0063
Oligonucleotides		
HK2 FW: TGCCACCAGACTAAACTAGACG	This paper	NA
HK2 RV: CCCGTGCCCACAATGAGAC	This paper	NA
GCLC FW: AGGACAAACCCAAACCATCCT	This paper	NA
GCLC RV: TGTTAAGGTACTGGGAAATGAAGT	This paper	NA
GPX3 FW: CCTTCCTACCCTCAAGTATGTCC	This paper	NA
GPX3 RV: AGGCGGTCAGATGTACCCA	This paper	NA

(*Continued on next page*)

Continued

REAGENT or RESOURCE	SOURCE	IDENTIFIER
LDHA FW: TTGACCTACGTGGCTTGGAAG	This paper	NA
LDHA RV: GGTAACGGAATCGGGCTGAAT	This paper	NA
ENO2 FW: AGCCTCTACGGGCATCTATGA	This paper	NA
ENO2 RV: TTCTCAGTCCCATCCAACTCC	This paper	NA
TKT FW: TCCACACCATGCGCTACAAG	This paper	NA
TKT RV: CAAGTCGGAGCTGATCTTCCT	This paper	NA
G6PD FW: ACCGCATCGACCACTACCT	This paper	NA
G6PD RV: TGGGGCCGAAGATCCTGTT	This paper	NA
ARG2 FW: CGCGAGTGCATTCCATCCT	This paper	NA
ARG2 RV: TCCAAAGTCTTTTAGGTGGCAG	This paper	NA
GATM FW: CACTACATCGGATCTCGGCTT	This paper	NA
GATM RV: CTAAGGGGTCCCATTCGTTGT	This paper	NA
HPRT FW: AGACTTTGCTTTCCTTGGTCAGG	This paper	NA
HPRT RV: GTCTGGCTTATATCCAACACTTCG	This paper	NA
GAPDH FW: CCCTTCATTGACCTCAACTACATG	This paper	NA
GAPDH RV: TGGGATTTCCATTGATGACAAGC	This paper	NA
CPS1 FW: AATGAGGTGGGCTTAAAGCAAG	This paper	NA
CPS1 RV: AGTTCCACTCCACAGTTCAGA	This paper	NA
AGMAT FW: GTGTGGTGCAGATTGGCATC	This paper	NA
AGMAT RV: GACCAGCAATTTCAGGTGTCC	This paper	NA
CKMT1B FW: ATATGACCCCCGGACAATGAA	This paper	NA
CKMT1B RV: CTTCGGCCAGTTCTGACTCT	This paper	NA
CKB esiRNA	Merck	EHU153971
KRAS esiRNA	Merck	EHU114431

RESOURCE AVAILABILITY

Lead contact

Further information and requests of reagents and resources should be directed to and will be fulfilled by the Lead Contact, Dr. Eros Di Giorgio (eros.digiorgio@uniud.it)

Materials availability

This study did not generate new unique reagents.

Data and code availability

- The RNA-seq data in this study have been deposited in the GEO database with the accession codes GSE217965, which is publicly available.
- This paper does not report original code.
- Any additional information required to reanalyse the data reported in this paper is available from the lead contact upon request.

EXPERIMENTAL MODEL AND STUDY PARTICIPANT DETAILS

The two human pancreatic adenocarcinoma cells, Panc-1 cells with a KRAS G12D (12 Gly→Asp) mutation (CVCL_0480) and MIA PaCa- 2 cells with a KRAS G12C (12 Gly→Cys) mutation (CVCL_0428), were genotyped by Microsynth (CH) to verify their identity. They matched 100% with the DNA profiles of the cell lines Panc-1 (ATCC® CRL-1469TM) and MIA PaCa-2 (ATCC® CRM-CRL-1420TM).”

The human embryonic cells Phoenix Ampho (CVCL_H716) and the human embryonic kidney cells HEK293T (CVCL_0063) were authenticated by morphology controls on the microscope and growth curve analysis. To ensure reliable and reproducible results, we keep the passage number of cells low. All cell lines were also tested for mycoplasma contamination before use.

METHOD DETAILS

Cell culture and reagents

Panc-1, MIA PaCa-2, HEK293T and Ampho cells were cultured in 10% FBS DMEM (Euroclone, Milan, Italy). All the cells were obtained from ATCC (Virginia, USA). Media were supplemented with 10 % FBS, L-glutamine (2 mM), penicillin (100 $U \cdot ml^{-1}$), and streptomycin (100 $\mu g \cdot ml^{-1}$) (Lonza, Basel, Switzerland). Low glucose DMEM was purchased from Euroclone (Milan, Italy). Arginine starvation medium was obtained from Thermo Fisher Scientific (SILAC DMEM Flex Media, A2493901), reconstituted with glucose, sodium pyruvate, glutamine and lysine (all from Merck, Milan, Italy). $NRF2^{-/-}$ knock-out was obtained by CRISPR/Cas9. Monoclonal cultures were grown in 96-well plate and validated by western-blotting and Sanger sequencing. Growth curves were obtained by seeding PDAC cells (30000 cells per well) in 12-well plate and allowed them to adhere overnight. Trypan Blue negative cells were counted every 2 days and medium culture was changed every 48 h. For the resazurin reduction assays, the cells were grown in 96-well plate for 120 min. at 37°C with resazurin solution (0.15 mg/ml) (Sigma-Aldrich, Milan, Italy). The fluorescence of the reduced product (resorufin) was quantified on a Perkin Elmer EnSpire 2300 Multilabel Reader (ex 550 nm/em 590 nm).

Plasmid construction, transfection, retroviral infection, silencing

Plasmid pWZL-HYGRO NRF2 was obtained by subcloning through a restriction-ligation based approach the ORF of NRF2 (BamHI/SalI) from pBABE HYGRO mRFP1 NRF2 (Addgene plasmid #136579). Are-luc was obtained by cloning the promotor region of NQO1 (-587 to -379) in pGL3 Basic plasmid (BglII/HindIII). pL NRF2 (-1810/+151) and pS NRF2 (-112/+151) were obtaining through a PCR-restriction based approach (NheI/BglII-BamHI). The plasmids encoding KRAS were obtained by inserting *KRAS* wt and *KRAS* G12D ORFs (NM_033360) into the HindIII/XhoI-restricted pcDNA3 plasmid using a PCR/restriction approach.

Transfections of 293 cells were carried out with polyethylenimine (PEI, 1μg/ml) using a 2:1 rate of PEI (μl): DNA (μg). Panc-1 cells were transfected with Lipofectamine 2000 (Thermo Fisher, Waltman, USA). siRNAs (74pmoles) were delivered by using Lipofectamine 3000 (Thermo Fisher, Waltman, USA). The following siRNAs were used: Ckb (esiRNA EHU153971, Merck); KRAS (esiRNA EHU114431, Merck). Retroviral infection was performed with M.O.I of 0.1-0.3 at 32°C by using Ampho cells as packaging cells.

Matrigel plug assay and spheroids culture

A total of 1600 cells were suspended in a Matrigel solution (20 μL 0.1% FBS-DMEM F-12, 60 μL Matrigel, Corning, USA) and plated on coverslips in 35-mm tissue culture plates. After 30 min of incubation at 37°C, the cells were fed with DMEM–20% FBS or DMEM low glucose 20% FBS. Following 4-day incubation, coverslips were fixed and stained with Phalloidin AF546 (Molecular Probes, Waltham USA) and Hoechst 33456 (Merck, Milan, Italy).

DMEM/F12 medium supplemented with 20% FBS or 0.1% FBS and 2.5% v/v reduced-growth factors Matrigel (Corning, USA) was used to grow PDAC spheroids.

Invasion assays

Each well of the invasion chamber (CLS3428, Corning, New York, NY, USA) was coated with 200 μL of Matrigel matrix coating solution (Cultrex, Trevigen, Gaithersburg, MD USA). Next, a cell suspension of 3×10^4 cells in 0.1 % FBS- DMEM or DMEM low glucose was added. As chemoattractant, 20 % FBS-DMEM was added in each lower chamber. As a control, 0.1 % FBS-DMEM was used to evaluate random invasion.

Cytofluorimetric analysis

ROS were quantified as follows: WT and $NRF2^{-/-}$ Panc-1 cells grown in adhesion for 2 days in 12-well plate were washed twice with PBS and incubated with 300 μl of 10 μM CM-H2DCFDA (Invitrogen, USA) for 30 min in phenol red-free DMEM without serum. To measure the mitochondrial membrane potential ($\Delta\Psi m$), 1×10^6 cells were loaded with 20 nM TMRM reagent solution (Life Technologies, UK) and incubated for 30 minutes at 37°C, 5% CO_2. In both cases, after two washings with PBS, the cells were harvested, resuspended in 200 μl PBS and single cell-suspensions were acquired in FL1 channel (ROS) and in FL2 channel (TMRM) at BD FACSCalibur flow cytometer equipped with a 488 nm argon laser.

ATP measurement, glutathione and total thiols assays

To measure ATP, WT and $NRF2^{-/-}$ Panc-1 cells grown in 35 mm plate and treated as reported in the text were lysed with 100 μl lysis buffer and processed accordingly to manufacturer (ab113849- Abcam). Luminescence was detected at GloMax 20/20 Luminometer (Promega, Madison, USA). Absolute quantification was achieved by comparison to ATP standard curve.

Reduced glutathione (GSH) was measured in cells grown in 96-well plate, lysed in 70 μl lysis buffer, deproteinized with 5-sulfosalicylic acid and processed accordingly to manufacturer (ab239709 Abcam). Absorbance was measured at O.D. 405 nm (EnSpire Multimode Plate Reader, PerkinElmer, Waltham USA). Total GSH was quantified as follows: GSH = (Slope sample -Slope blank)/Slope STD Curve.

For total thiols quantification, the cells grown in 96-well plate were incubated for 30 minutes with 50 μL of GSH reaction mixture at room temperature. Fluorescence intensity was recorded at Ex/Em = 490/520 nm (EnSpire Multimode Plate Reader, PerkinElmer, Waltham USA) and total thiols quantification was obtained through standard curve interpolation.

Immunofluorescence and immunoblotting

WT and *NRF2*$^{-/-}$ Panc-1 spheroids were fixed with 3 % paraformaldehyde and permeabilized with 0.3 % Triton X-100. Actin was labelled with phalloidin-AF546 (Molecular Probes, USA). Cells were imaged with a confocal microscope Leica TCS SP8X. Nuclei were stained with Hoechst 33342 (10 μg/ml, Merck). Images represent maximum intensity projections of 3D image stacks and were adjusted for brightness and contrast for optimal visualization.

Cell lysates after SDS-PAGE and immunoblotting on nitrocellulose (Whatman, UK) were incubated with primary antibodies that are listed in key resources table. Lysates from 3D culture were obtained by melting the matrix by incubating the plates in ice for 5 minutes after extensive washing in PBS. 0.1 ml Laemmli buffer 2x was used for each 3D sample. HRP-conjugated secondary antibodies were obtained from Cell Signalling (Danvers, USA) and blots were developed with Super Signal West Dura (Pierce, USA). For fluorescence-based detection, AF660 or AF760 secondary antibodies were used (Merck, Milan, Italy) and images were acquired at Odyssey M Imaging System (LI-COR Biosciences, USA).

Cell Mito Stress Test

The experiments have been carried out on XFe Extracellular Flux Analyzer (Seahorse, Agilent Technologies, Santa Clara, CA, USA). Briefly, 4x104 WT, *NRF2*$^{-/-}$ or *NRF2*$^{-/-}$ + NRF2 Panc-1 cells were seeded (5 replicates for each experiment) and cultured in XF Cell Culture Microplates (Agilent Technologies) in 500 μl complete DMEM medium and incubated for 24 h at 37 °C in 5% CO_2 atmosphere. Before the measurements, the culture medium was removed from each well and replaced with 500 μl of Seahorse XF Base Medium (Agilent Technologies), pre-warmed at 37 °C and supplemented with 10 mM glucose (Sigma-Aldrich, Heidelberg, Germany), 1 mM pyruvate (EuroClone, Milan, Italy), 2 mM glutamine (Sigma-Aldrich, Heidelberg, Germany), at pH 7.4. Cells were incubated in a CO2-free incubator at 37°C for 1 h and OCR (oxygen consumption rate) and ECAR (extracellular acidicication rate) were detected under basal conditions. The following compounds were prepared for each injection port to reach the final concentration of 1 μM oligomycin A, 0.5 μM FCCP, 0.5 μM rotenone and 0.5 μM antimycin A (Merck, Milan, Italy). Volumes of respectively 56, 62, 69 μl of compounds were added to each injection port. OCR values were normalized to the protein content (μg) quantified by spectrophotometry (Bradford assay, Euroclone, Milan, Italy).

Metabolite extraction and liquid chromatography–mass spectrometry of label-free metabolites

WT, *NRF2*$^{-/-}$ or *NRF2*$^{-/-}$ + NRF2 Panc-1 cells were plated in 10 cm plates and cultured in DMEM for 48 h. 1x10^7 cells of each condition were harvested, and cell pellets were washed twice with physiological solution and resuspended into 1 ml of 80 % methanol. Four biological replicates of WT, *NRF2*$^{-/-}$ and *NRF2*$^{-/-}$ cells re-expressing NRF2 were analyzed. All samples were lysed on a MM 400 mill mixer for 1 min three times, at a shaking frequency of 30 Hz and with the aid of two metal balls, followed by sonication in ice water bath for 2 min. The samples were centrifuged at 21000 g, 5°C for 10 min. The clear supernatants were used for the following LC-MS analyses and the protein pellets were used to measure protein content using a standardized Bradford assay procedure. For the analysis of fumaric acid, phosphocreatine and carbamoyl-P, metabolites were extracted with ice cold extraction buffer consisting of methanol, acetonitrile and water. A stock solution of the three targeted compounds was prepared in an internal standard solution of fumaric-d4 acid in 80 % acetonitrile. This solution was serially diluted with the same solution to have 8-point calibration solutions, in a range of 0.0001 to 10 nmol/ml for each compound. The clear supernatant of each sample solution was diluted 10 times with the internal standard solution. 10 μl aliquots of the calibration solutions and the sample solutions were injected into a HILIC column (2.1 x 100 mm, 1.8 μm) to run UPLC-MRM/MS with negative ion detection on a Waters Acquity UPLC coupled to a Sciex QTRAP 6500 Plus MS instrument, with the use of 5 mM ammonium acetate buffer and acetonitrile as the mobile phase for gradient elution (80% to 20% B in 10 min) at 30°C and 0.3 ml/min. A stock solution of the other compounds was prepared in internal standard solution in 80 % acetonitrile. This solution was serially diluted with the same internal standard solution to make 8-point calibration solutions, in a range of 0.0005 to 100 nmol/ml for each compound. The clear supernatant of each sample solution was diluted 10 times with the same internal standard solution. 10 μl aliquots of the calibration solutions and the sample solutions were injected into an Amide UPLC column (2.1 x 100 mm, 1.7 μm) to run UPLC-MRM/MS with positive ion detection on a Waters Acquity UPLC coupled to a Sciex QTRAP 6500 Plus MS instrument, with the use of 0.1 % formic acid and acetonitrile as the mobile phase for gradient elution (90 % to 30 % B in 12 min) at 30 °C and 0.35 ml/min. LC–MS analysis was performed at Creative Proteomics (Shirley, USA). For the analysis of the results, concentrations of the detected analytes were calculated with internal standard calibration by interpolating the constructed linear-regression curves of individual compounds, with the analyte-to-internal standard peak ratios measured from sample solutions, in an appropriate concentration range for each metabolite.

Polyamine quantification and arginine consumption rate

For polyamine quantification, PDAC cells were grown for 3 days in 60mm plates in complete DMEM. Cells were collected in 1ml of cold PBS by mechanical harvesting. After centrifugation, cells were lysed with 0.1 ml of ice-cold Polyamine Assay Buffer and incubated for 30' at 37°C with 0.002 ml of fluorescent polyamine probe (MAK349, ex/em 532/587) (Merck, Italy). Fluorescence was detected with Synergy H1 (Biotek, US). Polyamine quantification was determined from comparison with standard curve.

For arginine consumption assay, PDAC cells were grown for 2 days in 35mm plates in complete medium. Then cells were extensively washed and exposed to DMEM deprived of exogenous arginine supplementation for 1 or 3 days. The levels of arginine at day 0,1, 3 of

arginine starvation were quantified with L-Arginine Assay Kit (Merck, MAK370). The consumption was quantified accordingly to the following formula: [arginine at day 1 or 3 of starvation]/[arginine at day 0]*100.

RNA extraction and quantitative qRT-PCR

WT, *NRF2*$^{-/-}$ or *NRF2*$^{-/-}$ + NRF2 Panc-1 cells were lysed using Trizol (Invitrogen, USA). 1.0μg of total RNA was DNAse I treated (Ambion, USA) and retro-transcribed by using 100 units of M-MLV Reverse transcriptase (Life Technologies, USA) in the presence of 1.6 μM oligo(dT) and 4 μM Random hexamers (Euroclone, Milan, Italy). qRT-PCRs were performed using SYBR green technology (KAPA Biosystems). Data were analyzed by comparative threshold cycle (delta delta Ct ΔΔCt) using *HPRT* and *ACTB* as normalizer.

RNA-seq analysis and gene set enrichment analysis (GSEA)

WT and *NRF2*$^{-/-}$ Panc-1 cells were lysed using Tri Reagent (Molecular Research Center, USA). Total RNA was treated with DNAse I (NEB, USA) and purified with RNA Clean & Concentrator (Zymo Research, USA). RNA-seq poly A enriched transcripts library preparation and sequencing were performed at BMR-Genomics (Padua, Italy) following Illumina specifications. Quality control for raw sequencing reads was performed with FastQC (v0.11.9) (www.bioinformatics.babraham.ac.uk/projects/fastqc/) and MultiQC (v1.09). Alignment of reads was conducted with STAR (v2.5.3a),[59] using the human genome assembly GRCh38 with reference annotation; reads were assigned to a gene based on EnsEMBL annotations and via the STAR function "quantMode GeneCounts". Differential expression (DE) analysis was performed using gene raw counts, within the R/Bioconductor DESeq2 package.[60] We estimated the dispersion parameter for each library using the biological group dispersion. Principal component analysis was carried out with the plotPCA function from the DESeq2 package (v1.28.1). Genes with raw counts mean < 64 between each condition replicates were removed from the analysis. Differential expression analysis was performed using DESeq2 with Wald test for significance. We adjusted for multiple hypothesis testing by employing Benjamini-Hochberg correction at a false discovery rate (FDR) of 0.05. Genes with an absolute fold change ≥ 1 were considered as differentially expressed. Genes were annotated with package AnnotationHub (v2.20.2) utilizing Ensembl annotation 100 data. Functional annotation was performed on KEGG, Reactome slimGO and Gene Ontology databases with ClusterProfiler (v3.16.1) and ReactomePA (v1.32.0). Gene set enrichment analysis (GSEA) and the MSigDB database were used to investigate statistically relevant biological associations. Heatmaps were generated for each gene set and the expression of each gene was expressed as $\log_2$ (fold change) of NRF2(-/-) vs WT cell samples. The direct binding of NRF2 in proximity (± 5 kb) to the TSS of the identified genes were retrieved from Harmonizome dataset (https://maayanlab.cloud/Harmonizome/). For GSEA analysis in Figure 8, core enrichment was computed on the "top enriched" genes for each category. This signature was then launched for functional enrichment analysis by interrogating KEGG and MSigDB Hallmark databases (http://bioinformatics.sdstate.edu/go/). cBioPortal (https://www.cbioportal.org) was consulted for the analyzes in Figures 8F–8H.

QUANTIFICATION AND STATISTICAL ANALYSIS

For experimental data, Student *t*-test was employed. Mann–Whitney test was applied when normality could not be assumed. $P < 0.05$ was chosen as statistical limit of significance. For comparisons between more than two samples, Anova test was applied coupled to Kruskal–Wallis and Dunn's Multiple Comparison Test. For correlation between two variables, Pearson correlation or Spearman correlation were calculated for normal or non-normal distributions, respectively. SynergyFinder3.0 (https://synergyfinder.fimm.fi/synergy/20231011000613173221/) was used to evaluate synergism between 2a and cyclocreatine treatments in Panc-1 cells. Excel and GraphPad Prism were used for routineer analysis, R/Bioconductor packages for large data analysis and heatmap generation. We marked with *$P < 0.05$, **$P < 0.01$, ***$P < 0.001$. Unless otherwise indicated, all the data in the figures were represented as arithmetic means ± the standard deviations from at least three independent experiments.